A comparison of Langmuir turbulence parameterizations and key wave effects in a numerical model of the North Atlantic and Arctic Oceans

Alfatih Ali[a,b,*], Kai H. Christensen[b,e], Øyvind Breivik[b,d], Mika Malila[a], Roshin P. Raj[a], Laurent Bertino[a], Eric P. Chassignet[c], Mostafa Bakhoday-Paskyabi[a]

[a] *Nansen Environmental and Remote Sensing Center, Thormøhlensgate 47, 5006 Bergen, Norway*
[b] *Norwegian Meteorological Institute, Norway*
[c] *Center for Ocean-Atmospheric Prediction Studies, FL, USA*
[d] *Geophysical Institute, University of Bergen, Norway*
[e] *Department of Geosciences, University of Oslo, Norway*

ABSTRACT

Five different parameterizations of Langmuir turbulence (LT) effect are investigated in a realistic model of the North Atlantic and Arctic using realistic wave forcing from a global wave hindcast. The parameterizations mainly apply an enhancement to the turbulence velocity scale, and/or to the entrainment buoyancy flux in the surface boundary layer. An additional run is also performed with other wave effects to assess the relative importance of Langmuir turbulence, namely the Coriolis-Stokes forcing, Stokes tracer advection and wave-modified momentum fluxes. The default model (without wave effects) underestimates the mixed layer depth in summer and overestimates it at high latitudes in the winter. The results show that adding LT mixing reduces shallow mixed layer depth (MLD) biases, particularly in the subtropics all year-around, and in the Nordic Seas in summer. There is overall a stronger relative impact on the MLD during winter than during summer. In particular, the parameterization with the most vigorous LT effect causes winter MLD increases by more than 50% relative to a control run without Langmuir mixing. On the contrary, the parameterization which assumes LT effects on the entrainment buoyancy flux and accounts for the Stokes penetration depth is able to enhance the mixing in summer more than in winter. This parameterization is also distinct from the others because it restrains the LT mixing in regions of deep MLD biases, so it is the preferred choice for our purpose. The different parameterizations do not change the amplitude or phase of the seasonal cycle of heat content but do influence its long-term trend, which means that the LT can influence the drift of ocean models. The combined impact on water mass properties from the Coriolis-Stokes force, the Stokes drift tracer advection, and the wave-dependent momentum fluxes is negligible compared to the effect from the parameterized Langmuir turbulence.

1. Introduction

The interaction between surface waves and ocean circulation is a complex process which involves a wide range of temporal and spatial scales, ranging from fast-moving waves to the much slower mean flow. The influence of wind-driven surface waves on the underlying ocean circulation and upper-ocean mixing has been recognized to play a critical role in reducing known systematic biases in climate models as discussed by Belcher et al. (2012), who argued that turbulent mixing in the ocean surface boundary layer will be underestimated if the effect of surface waves is not accounted for. The feedback to the atmosphere is mostly thermodynamic, and a relatively small temperature bias may

have large consequences for the deep convection in the atmosphere (Sheldon and Czaja, 2014). The ocean primary production is also strongly influenced by the thickness of the mixed layer, and therefore accurate predictions of the mixed layer depth (MLD) are crucial for biogeochemical modeling.

Neglecting the near-surface effects of whitecapping, the main impact of surface waves on upper-ocean dynamics is broadly believed to be related to an aggregate drift of water particles known as the Stokes drift (Stokes, 1847). The interaction between the Stokes drift and the mean current vorticity forces overturning cell-like structures known as Langmuir circulation cells (Leibovich, 1983; Thorpe, 2004), which interact with a multitude of small-scale processes in the oceanic boundary

---

layer to produce a turbulence regime called Langmuir turbulence (LT) (McWilliams et al., 1997; Ardhuin and Jenkins, 2006; Suzuki and Fox-Kemper, 2016).

The oceanic momentum balance is affected by an enhanced veering (compared to Ekman veering) of the currents due to the Coriolis-Stokes force (Hasselmann, 1971; Weber, 1983) and the advection of tracers by the Stokes drift (e.g., van den Bremer and Breivik, 2018), as well as by the interaction of the Stokes shear with the Eulerian advection of momentum (McWilliams and Restrepo, 1999; Suzuki et al., 2016). The latter effect is traditionally represented in the form of a so-called vortex force theory and a modified pressure term, following the asymptotic theory developed by Craik and Leibovich (1976) to explain Langmuir circulation. Although potentially important in coastal regions (e.g., Uchiyama et al., 2010), the significance of the Craik-Leibovich vortex force on the large-scale ocean circulation has been questioned on the basis of the higher-order nature of the terms in the wave phase-averaged momentum equations (Mellor, 2016).

The importance of the inclusion of surface wave effects such as Langmuir turbulence mixing in general circulation models has been given more attention recently (Belcher et al., 2012; Fan and Griffies, 2014; Breivik et al., 2015; Noh et al., 2016; Li et al., 2016, 2017). Downwelling jets associated with Langmuir circulation may penetrate beyond the Stokes depth (Polton and Belcher, 2007), and can therefore increase the turbulent mixing down to the base of the surface boundary layer, enhancing the deepening of MLD (Li et al., 1995; Sullivan et al., 2007). The downward velocity associated with Langmuir cells significantly energizes buoyancy-driven overturning circulations at sub-mesoscale fronts when they are aligned with the Stokes shear (Suzuki et al., 2016).

Large eddy simulation (LES) studies of the Langmuir circulation using the vortex force have shown considerable enhancement of the turbulent kinetic energy (TKE) in the surface boundary layer (e.g Skyllingstad and Denbo, 1995; McWilliams et al., 1997; Sullivan et al., 2007; McWilliams and Fox-Kemper, 2013). In an investigation to quantify the impact, D'Asaro et al. (2014) found an average increase of 15–20 % in MLD at high latitudes, as well as enhancement of the vertical turbulent kinetic energy (VKE) within the mixed layer by approximately a factor of two. Using LES solutions of the wave-averaged equations in a weakly convective, wind driven surface boundary layer, McWilliams and Sullivan (2000) (hereafter MS00) were the first to propose a parameterization of the bulk effects of LT in the *K*-Profile Parameterization turbulence scheme (KPP) (Large et al., 1994) using the turbulent Langmuir number

$$\mathrm{La_t} = [u^*/v^s(0)]^{1/2} \tag{1}$$

of McWilliams et al. (1997). Here, u^* and $v^s(0)$ are the water-side friction velocity and surface Stokes drift, respectively. The turbulent Langmuir number, $\mathrm{La_t}$, can be understood as a measure of the production of the turbulence kinetic energy by current shear relative to the Stokes drift production (Grant and Belcher, 2009). MS00 themselves noted that their parameterization lacks an explicit stability dependence, suggesting that it may not be applicable in realistic applications without further modifications. To address this limitation, Smyth et al. (2002) (hereafter Sm02) extended the MS00 formula to include stratification effects intended to restrain the mixing enhancement under unstable stratification, i.e. in convective conditions, and to magnify it under stable stratification.

Harcourt and D'Asaro (2008) reformulated the Langmuir number in terms of a surface layer averaged value of the Stokes drift instead of its surface value and have shown it to be successful in capturing the bulk properties of the VKE in the mixed layer. The surface layer averaged Langmuir number is given as

$$\mathrm{La_{SL}} = [u^*/(\langle v^s \rangle_{SL} - v^s_{ref})]^{1/2} \tag{2}$$

where $\langle v^s \rangle_{SL}$ represents the Stokes drift magnitude averaged over a thin layer near the surface and its thickness is estimated as the top 20% of

the ocean mixed layer (Harcourt and D'Asaro, 2008), and v^s_{ref} is the Stokes drift at a reference level considered to be at the base of the mixed layer. The averaging over the thin surface layer is introduced to address the importance of the Stokes decay scale in influencing the structure and the dynamics of LT. The surface layer-averaged Langmuir number (2) has recently been shown to yield good results in the LT-induced mixing enhancement in several studies (Harcourt and D'Asaro, 2008; Van Roekel et al., 2012; Reichl et al., 2016b; Li et al., 2016).

Takaya et al. (2010) (hereafter Tk10) proposed a refinement of a prognostic skin SST model by accounting for Langmuir turbulence mixing under stable conditions using a velocity scale by Grant and Belcher (2009). Although they did not test it in KPP, they followed the MS00 approach and proposed the scaling by Grant and Belcher (2009) as an LT enhancement factor applied to the eddy diffusivity in their SST model in such way that it neglects the LT effects under large values of $\mathrm{La_t}$. They have shown it to be successful in enhancing ocean mixing and reducing the diurnal variability of SST under waves presence.

Van Roekel et al. (2012) (hereafter VR12), using a broadband empirical wave spectrum, introduced Langmuir mixing parameterization accounting for the misalignment between wind and wave directions, which is also based on a surface layer-averaged Langmuir number. Here, we use their adjusted enhancement factor for the conditions where wind and waves are aligned (Li et al., 2016). In addition, we adopt the LT enhancement of the boundary layer entrainment by modifying the bulk Richardson number with a Stokes drift term (Li et al., 2016).

Li and Fox-Kemper (2017) (hereafter LF17) investigated the LT effects on the entrainment buoyancy flux in the ocean surface boundary layer using LES with various combinations of wind, waves and (destabilizing) surface buoyancy flux. It is found that the entrainment is enhanced substantially under weakly convective conditions, while the effects are moderate under strongly convective turbulence. They therefore proposed an LT enhancement estimate of the scaling of the entrainment buoyancy flux at the base of the boundary layer, and derived a new expression for the unresolved turbulence shear velocity in the KPP scheme. Combined with a $\mathrm{La_{SL}}$-based enhancement factor from Van Roekel et al. (2012), they have shown that this new modification has improved the MLD in the southern ocean in their Community Earth System Model (CESM) model simulations.

There have been recent studies where Langmuir mixing parameterizations in KPP have been compared in global climate simulations, for example Fan and Griffies (2014) and Li et al. (2016) using, respectively, the Geophysical Fluid Dynamics Laboratory (GFDL) Climate Model (CM2M) and CESM. Both are coupled with WAVEWATCH III (Tolman et al., 2002; Tolman and Others, 2009). The ocean components for CM2 M and CESM are the Modular Ocean Model (MOM4) and the Parallel Ocean Program (POP2), respectively. Fan and Griffies (2014) found the MS00 parameterization to cause excessive mixing and the Sm02 scaling to work best in correcting warm SST and shallow MLD biases in CM2M. However, Li et al. (2016) found both parameterizations to induce too much mixing, suggesting that the effect could be model dependent. This motivated them to test with the parameterization from Van Roekel et al. (2012), considering surface-layer averaged Langmuir number, wind-wave misalignment, as well as boundary layer entrainment enhancement, finding these to introduce substantial improvements in MLD predictions in the southern ocean in the summer.

In this study, we assess the impact of five parameterizations of LT mixing in the KPP scheme implemented in the HYbrid Coordinate Ocean Model (HYCOM) (Bleck, 2002), described above as MS00, Sm02, Tk10, VR12 and LF17 with enhancement factors based on the Langmuir numbers $\mathrm{La_t}$ or $\mathrm{La_{SL}}$, and in the case of the Sm02 and LF17 parameterizations, also the stability. The wave forcing fields are interpolated from a WAVEWATCH III global hindcast (Rascle et al., 2008; Rascle and Ardhuin, 2013).

Langmuir turbulence is considered to be an important wave-related mixing process (Belcher et al., 2012) in the open ocean. In order to

assess its impact relative to other wave effects we have included one experiment, CSFSm02, where we add the Coriolis-Stokes force (Hasselmann, 1970), the tracer advection by the Stokes drift (Uchiyama et al., 2010), and the wave-modified stress. The latter is a consequence of the growth and decay of waves with changing winds because waves absorb a portion of the wind stress when they grow, and conversely the momentum flux to the ocean from breaking waves continues after the wind has died down (Weber, 1983; Janssen, 2012; Breivik et al., 2015).

A regional configuration of HYCOM for the North Atlantic and the Arctic Ocean is used here, referred to as TOPAZ4 (Sakov et al., 2012), which is providing both the Arctic forecast and reanalysis products of the Copernicus Marine Environment Services (CMEMS). We will try to reconcile the results from previous comparison studies and suggest a practical operational implementation able to improve the TOPAZ4 forecast and reanalysis services for CMEMS. To our knowledge this study is the first time these parameterizations have been compared in a realistic basin-scale ocean model.

As will be shown, we find improvements in the reduction of the warm SST and shallow MLD biases with Langmuir mixing in the subtropical summer with Sm02, VR12 and LF17 parameterizations. However, the Sm02 and VR12 scalings appear to degrade the wintertime MLD leading to increased root-mean-square errors (RMSE) at high latitudes. The Tk10 scaling is also found to reduce MLD and SST biases, however it appears to introduce an excessive mixing that causes too high heat content and MLD deepening. In agreement with the findings by Fan and Griffies (2014) and Li et al. (2016) we also find the parameterization by MS00 to introduce the most vigorous mixing. The control run without LT effects yields a too deep mixed layer at mid/high latitudes and underpredicted SSTs in the middle of the North Atlantic. These biases (in the control run) are found to be exacerbated when adding Langmuir mixing, particularly with the parameterization of MS00. In agreement with the finding by Li and Fox-Kemper (2017), the LT-enhanced unresolved shear with the LF17 approach is found to restrain the MLD deepening induced by VR12 parameterization in which the Stokes drift term $v^s(0)^2$ is added to the denominator of the bulk Richardson number. Furthermore, the mixing enhancement with the surface layer averaged Langmuir number used in LF17 is shown to reduce the LT effects in regions that already overestimate the winter MLD, while it increases it during summer. Among the LT parameterizations considered here, the LF17 scheme is found to reduce the summer MLD RMSEs the most. It also performs as good as the control run during winter.

This paper is organized as follows. A description of the methodology is given in Section 2, where the wave-averaged equations, the Stokes drift profile approximation, and the parameterization of the Langmuir turbulence mixing are outlined. In Section 3, the results of in total seven experiments, as well as a comparison against observations, are presented, with a focus on the influence on ocean temperature, total heat content and mixed layer depth. The results are discussed and summarized in Section 4.

2. Methodology

In the present study, HYCOM is configured for a domain covering the North Atlantic and Arctic Oceans ranging from 10 km and 16 km horizontal resolution (from 1/6 to 1/8˚) and forced with wind fields from the ERA-Interim reanalysis (Dee et al., 2011) of the European Centre for Medium-Range Weather Forecasts (ECMWF). There are 50 hybrid vertical layers, of which 10 are fixed z layers covering approximately the upper 20 m. The model setup is similar to Sakov et al. (2012) except that data assimilation is not included, and the vertical resolution has been increased from 28 to 50 hybrid layers. In addition, the thickness of the top layer is set to 1 m rather than 3 m, which is important, in particular for the Coriolis-Stokes force and the Stokes tracer advection, since the Stokes drift decays rapidly with depth. At the lateral boundary the model variables are relaxed towards the

corresponding monthly climatology using relaxation zones of width equivalent to 20 grid cells. In addition a barotropic inflow is imposed through the Bering Strait to account for the inflow of Pacific Water. This, however, is balanced by an equivalent outflow at the southern open boundary. The thermodynamics fluxes are determined following Drange and Simonsen (1996), and to better represent the diurnal cycle, the estimation of the short wave radiation is updated every three hours.

The integrated wave parameters are computed from the full wave spectrum, where the wave effects on sea ice are neglected. The wind forcings used in the wave hindcast are from a combination of ECMWF operational analyses and the Climate Forecast System Reanalysis (Saha et al., 2010). The Stokes drift profile is reconstructed based on the Phillips spectrum approximation, following Breivik et al. (2016) and Li et al. (2017).

Here a brief description of the wave-averaged equations and the Langmuir turbulence mixing parameterizations in the KPP scheme are given. At the end of this section, the Stokes drift profile approximation is presented, as well as a description of the experimental setup and the observations used for model validation.

2.1. Wave terms in the mean flow equations

The Stokes drift (Stokes, 1847) is defined as the difference between the mean Eulerian velocity at a fixed point ($\mathbf{u}$,w) and the mean Lagrangian velocity ($\mathbf{u}_L$,w_l) of a particle subjected to an orbital motion (Andrews and Mcintyre, 1978; van den Bremer and Breivik, 2018), and given by the relation

$$(\mathbf{u}_L, w_l) = (\mathbf{u}, w) + (\mathbf{U}^s, W^s) \quad . \tag{3}$$

The implementation of the wave-averaged equations in HYCOM, following the vortex force formalism based on the generalized Lagrangian mean (GLM, (see Andrews and Mcintyre, 1978; Ardhuin et al., 2008)) approach, is reported by Rogers and Wallcraft (2013). The GLM equations of Ardhuin et al. (2008), are also presented more explicitly in Bennis et al. (2011). In an Eulerian frame of reference, and using the asymptotic theory in which the relation (3) is valid, the wave-averaged equations (Craik and Leibovich, 1976; McWilliams and Restrepo, 1999; McWilliams et al., 2004; Uchiyama et al., 2010), are

$$\frac{\partial u}{\partial t} + (\mathbf{u} \cdot \nabla_h)u + w\frac{\partial u}{\partial z} - fv + \frac{1}{\rho}\frac{\partial p}{\partial x} - F_{m,x} = \left(f + \left[\frac{\partial v}{\partial x} - \frac{\partial u}{\partial y}\right]\right)V^s$$
$$- W^s\frac{\partial u}{\partial z} - \frac{\partial J}{\partial x} + F_{w,x} \quad ,$$

$$\frac{\partial v}{\partial t} + (\mathbf{u} \cdot \nabla_h)v + w\frac{\partial v}{\partial z} + fu + \frac{1}{\rho}\frac{\partial p}{\partial y} - F_{m,y} = -\left(f + \left[\frac{\partial v}{\partial x} - \frac{\partial u}{\partial y}\right]\right)U^s$$
$$- W^s\frac{\partial v}{\partial z} - \frac{\partial J}{\partial y} + F_{w,y} \quad ,$$
$$\tag{4}$$

where ∇_h is the horizontal differential operator, and ($\mathbf{U}^s \equiv (U^s,V^s),W^s$) and ($\mathbf{u} \equiv (u,v),w$) represent the 3D Stokes and mean Eulerian velocities, respectively. The water density is represented by ρ and the hydrostatic pressure as p. The terms ($F_{m,x},F_{m,y}$) represent the non-wave source of momentum diffusion and mixing effects, J denotes Bernoulli head, and ($F_{w,x},F_{w,y}$) is the wave-induced non-conservative force due to for example wave breaking or dissipation due to ocean bottom friction. The vortex force, including the Coriolis-Stokes force $f\hat{\mathbf{z}} \times \mathbf{U}^s$, is given by the first two terms on the right hand side in Eq. (4).

At the surface the boundary condition is modified by the presence of surface waves which reduce the momentum injected to the ocean when they grow, and conversely release momentum when they break and dissipate. Therefore the wind stress τ_a is modified by subtracting the part absorbed by wave generation or the atmospheric-to-wave momentum flux τ_{aw}. At the same time, the wave-to-ocean momentum flux τ_{wo} due to wave breaking is added as an additional stress. Hence the

ocean-side stress τ_{oc}, following Jenkins (1989), Weber et al. (2006) and Janssen (2012), is expressed as

$$\tau_{oc} = \tau_a - (\tau_{aw} - \tau_{wo}) \quad , \tag{5}$$

where

$$\tau_{aw} = \rho g \int_0^{2\pi} \int_0^\infty \frac{\mathbf{k}}{\omega} S_{in} \quad d\omega \quad d\theta \qquad \text{and}$$

$$\tau_{wo} = \rho g \int_0^{2\pi} \int_0^\infty \frac{\mathbf{k}}{\omega} S_{diss} \quad d\omega \quad d\theta, \tag{6}$$

here S_{in} is the wind input source function, S_{diss} is the wave dissipation source term, $\mathbf{k}$ is the wave number, ω the angular wave frequency and θ is the wave direction. The transport equation for a tracer C, with Stokes advection ($\mathbf{U}^s \cdot \nabla_h$), is given in the form (Uchiyama et al., 2010)

$$\frac{\partial C}{\partial t} + (\mathbf{u} \cdot \nabla_h)C + w\frac{\partial C}{\partial z} = -(\mathbf{U}^s \cdot \nabla_h)C - W^s\frac{\partial C}{\partial z}$$
$$+ \nabla_h \cdot (\nu \nabla_h C) + \frac{\partial}{\partial z}\left(\nu_z \frac{\partial C}{\partial z}\right), \tag{7}$$

where (ν, ν_z) are the horizontal and vertical turbulent diffusion coefficients, respectively. As the main focus of this study is the Langmuir mixing, we only include the Coriolis-Stokes force, the Stokes tracer advection and the wave-dependent stress in one experiment (CSFSm02) to assess the importance of these effects relative to the impact of Langmuir turbulence.

General ocean circulation models are mainly assumed hydrostatic typically with $O(10\,\text{km})$ horizontal grid resolution, while turbulence mixing is due to non-hydrostatic processes of $O(1\,\text{m})$ scales. These small scale-processes must thus be parameterized with turbulence closure schemes. An essential goal of these schemes is to produce accurate and efficient parameterizations of the vertical mixing in large-scale circulation models. An example of such turbulence schemes is the non-local K-profile parameterization (KPP) (Large et al., 1994), which provides a reasonable compromise between computational efficiency and resolving boundary layer physics. Here, a number of LES-based parameterizations proposed to capture the sub-grid scale effects of the Langmuir turbulence in KPP are investigated.

2.2. Langmuir mixing parameterization in KPP

In the KPP scheme (Large et al., 1994), the parameterization of the turbulent fluxes requires splitting the water column into two regions, the surface boundary layer and the ocean interior, each of which has a distinct mixing regime. The ocean surface boundary layer depth (not MLD) is defined as the shallowest depth $h(t)$ at which the bulk Richardson number $Ri_b(z)$ reaches a critical number Ri_c (here considered to be 0.3), where $Ri_b(z)$ is defined as

$$Ri_b(z) = \frac{(B_r - B(z))|z|}{|\mathbf{u}_r - \mathbf{u}(z)|^2 + V_t^2(z)}. \tag{8}$$

Here V_t represents the unresolved turbulent velocity shear, while B_r is the buoyancy and $\mathbf{u}_r$ the velocity, both averaged over a thin surface layer. Large et al. (1994) define the MLD as the shallowest depth at which the buoyancy gradient exceeds a threshold, and thus their MLD in most cases is smaller than the boundary layer depth h. The unresolved turbulence shear is parameterized (Large et al., 1994) by the relation

$$V_t^2(z) = \frac{C_v N(z) w_s |z|}{Ri_c \kappa^2} \left(\frac{-\beta_T}{c_s \epsilon}\right)^{\frac{1}{2}}, \tag{9}$$

where $C_v = \max(2.1 - 200.0 \times \max(0, N), 1.7)$ (Danabasoglu et al., 2006), w_s is the turbulence velocity scale for scalar properties, $N(z)$ is the local buoyancy frequency, $\kappa = 0.4$ is the von Kármán constant, and $c_s = 98.96$ and $\epsilon = 0.1$. The parameter β_T represents the ratio of the entrainment buoyancy flux $-\overline{w'b_e'}$ at the base of the boundary layer to the surface buoyancy flux which is considered to be approximately a constant (here $\beta_T = -0.2$) under pure convection (Large et al., 1994).

The turbulent flux of a property X is parameterized by

$$\overline{x'w'} = -K_x \left(\frac{\partial X}{\partial z} - \gamma_x\right) \quad , \tag{10}$$

here γ_x represents a non-local transport (Large et al., 1994), which is assumed to be non-zero only for scalar variables in unstable regimes. Within the surface boundary layer, $0 < |z| < h$, the turbulent eddy diffusivity/viscosity is parameterized as

$$K_x(z, t) = h(t) w_x(z/h, t) G(z/h) \quad , \tag{11}$$

where G is a smooth shape function assumed to be a cubic polynomial, and the subscript x refers to a scalar or momentum property. The turbulence velocity scale is given as $w_x = \kappa u^*/\phi$, where u^* is the friction velocity and ϕ is the stability function defined by Large et al. (1994).

With the aid of LES simulatins of the wave averaged equations, McWilliams and Sullivan (2000) proposed a parameterization of the bulk effects of LT mixing in KPP by applying an enhancement factor $\mathcal{E}(La_t)$ to the turbulence velocity scale within the surface boundary layer as

$$w_x = \frac{\kappa u^*}{\phi} \mathcal{E}(La_t) \quad . \tag{12}$$

Which means that the LT enhancement factor is applied to the velocity scale for both scalar and momentum quantities, enhancing both the unresolved shear and the eddy diffusivity. The enhancement factor proposed by McWilliams and Sullivan (2000) has the form

$$\mathcal{E}(La_t) = \left[1 + \frac{C_w}{La_t^{2\alpha}}\right]^{1/\alpha} \quad , \tag{13}$$

where C_w and α are assumed positive constants. In cases with small turbulent Langmuir numbers, the turbulence velocities become proportional to the surface Stokes drift, and in the limit of $La_t \to \infty$, the enhancement factor becomes unity, meaning that the TKE production is dominated by current shear production. In addition to amplifying the mixing, the enhanced turbulence velocity scale will also deepen the boundary layer h through increasing the unresolved shear velocity in the denominator of the bulk Richardson number (8). McWilliams et al. (2014) also suggest that the expression for V_t^2 should include the effects of the unresolved LT on the boundary layer thickness. In the default KPP implementation in HYCOM, the mixing coefficients at the boundary layer depth h are matched with those of the interior. Thus, the mixing in the interior can influence the mixing within h.

In the following subsections, we look at the choice of the enhancement factor suggested for each of the five LT parameterizations considered in this study.

2.2.1. McWilliams and Sullivan (2000) parameterization (MS00)

From their LES experiments of the wave-averaged equation on a weakly convective, quasi-equilibrium turbulent state, MS00 proposed an enhancement factor in the form

$$\mathcal{E}(La_t) = \left[1 + \frac{0.080}{La_t^4}\right]^{1/2} \quad , \tag{14}$$

which they found to give better agreement with their LES results. Their LES model was forced by a uniform wind stress and monochromatic surface waves. However, MS00 admitted that their definition lacks an explicit stability dependency on the convective forcing, suggesting that their proposed generalization of the KPP model may not be applicable in a full range of realistic oceanic conditions without further modifications.

2.2.2. Smyth et al. (2002) parameterization (Sm02)

Based on analyses of LES experiments and observational data of strongly stable (daytime warming) and strongly unstable (nocturnal cooling) forcing conditions, Smyth et al. (2002) proposed an extension

to the MS00 scaling incorporating a dependence on the convective velocity scale, $w^* = (-B_f h)^{1/3}$, where B_f is the surface buoyancy flux. The proposed modification makes C_w, which was assigned a constant value of 0.08 in MS00's formulation, a function of w^* and the friction velocity, u^*, such that the influence of the Langmuir mixing is restrained under destabilizing surface forcing ($B_f < 0$) and is enhanced under stabilizing conditions ($B_f > 0$). The extended formulation, therefore, takes the form

$$\mathcal{E}(\text{La}_t) = \left[1 + \frac{C_w(u^*, w^*)}{\text{La}_t^4} \right]^{1/2} \quad , \tag{15}$$

where $C_w(u^*, w^*) = 0.15 \left[\frac{u^{*3}}{u^{*3} + 0.6 w^{*3}} \right]^2$ ensures that the enhancement is prevented from attaining unreasonably high levels in strongly convective conditions. In addition, Smyth et al. (2002) proposed non-local momentum fluxes, however these are not considered here (following Large et al. (1994) as well as Fan and Griffies (2014)).

2.2.3. Takaya et al. (2010) parameterization (Tk10)

Takaya et al. (2010) modified a prognostic skin SST scheme developed by Zeng and Beljaars (2005) to include a surface wave-dependence under stable (surface warming) forcing conditions, in which the standard scheme has been found to overestimate the surface temperature. Whereas the original scheme parameterized the thermal diffusivity in terms of classical Monin-Obukhov similarity theory, the Tk10 modification adds an La_t-dependent enhancement factor to the diffusivity formula as

$$\mathcal{E}(\text{La}_t) = \max(1, \text{La}_t^{-2/3}) \quad . \tag{16}$$

Here, the Langmuir enhancement function $\mathcal{E}(\text{La}_t)$ is defined so that it does not affect the mixing for large La_t, and is made to fit with the Langmuir turbulence velocity scaling by Grant and Belcher (2009). Tk10 found that including the impact of Langmuir turbulence (in terms of increased mixing) improved the model's representation of the diurnal SST variability.

Although not originally designed to parameterize Langmuir turbulence in the KPP mixing scheme, the LT enhancement function of Tk10 has been implemented in the HYCOM version of KPP in an equivalent manner to the previously described parameterizations, i.e. as a multiplicative enhancement factor for the unresolved turbulent vertical velocity, w_x.

2.2.4. Van Roekel et al. (2012) parameterization (VR12)

The parameterization by Van Roekel et al. (2012) takes into account a possible mismatch in the direction between waves and the wind (neglected in this work), and has been tested in global simulations by Li et al. (2016). It was found to show the optimal MLD improvement when combined with an enhancement of the boundary layer entrainment, specially in the Southern Ocean. Assuming that wind and waves are aligned and hence the definition of La_t as a function of only u^* and $v^s(0)$, the enhancement factor (Van Roekel et al., 2012; Li et al., 2016) used in this study takes the from

$$\mathcal{E}(\text{La}_t) = [1 + (3.1\text{La}_t)^{-2} + (5.4\text{La}_t)^{-4}]^{\frac{1}{2}} \quad . \tag{17}$$

Modification of the parameterization of the boundary layer in KPP following Li et al. (2016) proposes an enhancement of the entrainment at the base of the surface boundary layer by adding the Stokes speed term to account for the Lagrangian current in the definition of the bulk Richardson number as

$$\text{Ri}_b(z) = \frac{(B_r - B(z))|z|}{|\mathbf{u}_r - \mathbf{u}(z)|^2 + V_t^2(z) + v^s(0)^2} \quad . \tag{18}$$

This entrainment enhancement is combined with the Van Roekel et al. (2012) scaling (17) and simply referred to as VR12 (see Table 1). However, to avoid double counting, it should be noted that the LT

Table 1

The six experiments of the LT mixing enhancement that have been considered in this study. The second column refers to both the corresponding scaling and numerical experiment. The surface Stokes drift square added to V_t^2 in VR12 is for the Lagrangian shear. Note that, to avoid double counting of the LT effects, the enhancement factor of VR12&LF17 is not applied to the velocity scale which appears in the expression for the unresolved shear. The control run (Cntl) is the case without including wave effects.

Parameterization	Exp.	Enhancement factor	Unresolved shear
Large et al. (1994)	Cntl	1	V_t^2
McWilliams and Sullivan (2000)	MS00	$\sqrt{1 + 0.080\text{La}_t^{-4}}$	V_t^2
Smyth et al. (2002)	Sm02	$\sqrt{1 + 0.15\left[\frac{u^{*3}}{u^{*3}+0.6w^{*3}}\right]\text{La}_t^{-4}}$	V_t^2
Takaya et al. (2010)	Tk10	$\max(1, \text{La}_t^{-2/3})$	V_t^2
Van Roekel et al. (2012)	VR12	$\sqrt{1 + (3.1\text{La}_t)^{-2} + (5.4\text{La}_t)^{-4}}$	$V_t^2 + (v^s(0))^2$ [1]
Li and Fox-Kemper (2017)	LF17	$\sqrt{1 + (1.5\text{La}_{SL})^{-2} + (5.4\text{La}_{SL})^{-4}}$	V_{tL}^2 [2]

[1] See Eq. (18)
[2] See Eq. (20)

enhancement factor Eq. (17) is not applied to the velocity scale w_s appearing in the expression for the unresolved shear Eq. (9). The enhancement of the boundary layer entrainment by Langmuir turbulence is found to elevate the deepening effects of the VR12 parameterization (Li et al., 2016).

2.2.5. Li and Fox-Kemper (2017) parameterization (LF17)

Motivated by the work of Li et al. (2016), with respect to parameterization of the LT influence on the boundary layer entrainment, Li and Fox-Kemper (2017) proposed a scaling to the entrainment buoyancy flux $-\overline{w'b'}_e$ to account for the effect of LT under a destabilizing surface buoyancy flux. In the derivation leading to the expression (9) for the unresolved shear in the default KPP, the entrainment buoyancy flux is parameterized using the empirical relation $-\overline{w'b'}_e = \beta_T B_f$ under pure convection (Large et al., 1994). To account for the Langmuir turbulence effects, Li and Fox-Kemper (2017) proposed that the entrainment buoyancy flux, under unstable conditions, scales as

$$\frac{-\overline{w'b'_e}h}{u^{*3}} = 0.17 + 0.083\text{La}_{SL}^{-2} - 0.15\frac{h}{\kappa L}, \tag{19}$$

where $L = u^{*3}/(\kappa B_f)$ is the Monin-Obukhov length. For the constants appearing in the right hand side, see Li and Fox-Kemper (2017), their Fig. 8b and Eq. (21) (also suggested through personal communication with the authors). Then the unresolved shear given in Eq. (9) is re-derived (Li and Fox-Kemper, 2017) to incorporate the new LT-enhanced entrainment buoyancy flux (19) as:

$$V_{tL}^2(z) = \frac{C_v N(z) w_s(z)|z|}{\text{Ri}_c} \left[\frac{-\overline{w'b'_e}h}{w_s(z)^3} \right]^{\frac{1}{2}} . \tag{20}$$

Note that this modified turbulent shear by Li and Fox-Kemper (2017) is applied only under destabilizing surface buoyancy flux, because this is the regime in which their LES simulations were conducted. Under neutral and stabilizing regimes, we apply the default unresolved turbulence shear given in Eq. (9). As illustrated by Li and Fox-Kemper (2017), the modified unresolved turbulence shear velocity V_{tL}^2 will make the diagnosed surface boundary layer slightly shallower in the convection limit, as V_{tL}^2 becomes slightly smaller than the default V_t^2. However, it will have deepening effects in the weak surface cooling limit, see Li and Fox-Kemper (2017), p 2877. This means that the deepening effect will be constrained under pure convection conditions (dominant winter conditions for example in the Labrador sea), while it will be enhanced under weak surface cooling and in the presence of

wind and waves.

In experiment LF17, in addition to including LT effects in the entrainment buoyancy flux in Eq. (19), and hence adopting the modified unresolved shear in Eq. (20), the $\mathrm{La_{SL}}$-based enhancement factor (Van Roekel et al., 2012; Li et al., 2016)

$$\mathcal{E}(\mathrm{La_{SL}}) = [1 + (1.5\mathrm{La_{SL}})^{-2} + (5.4\mathrm{La_{SL}})^{-4}]^{\frac{1}{2}} \tag{21}$$

is applied to the velocity scale w_x of the turbulence eddy diffusivity in Eq. (11). It is assumed that the LT affects both the entrainment buoyancy flux and the eddy diffusivity. However, to avoid double counting, it should be noted that the LT enhancement factor (21) is not applied to the velocity scale appearing in the expression for the unresolved shear (20). Note also that here the Stokes drift term is not added in the denominator of the bulk Richardson number (see Table 1).

2.3. Estimating the Stokes drift velocity profile

In deep water, the Stokes drift velocity profile is computed from the two-dimensional wave spectrum $E(\omega,\theta)$ as

$$\mathbf{U}^s(z) = \frac{2}{g} \int_0^{2\pi} \int_0^\infty \omega^3 \hat{\mathbf{k}} e^{2kz} E(\omega, \theta) \, d\omega \, d\theta , \tag{22}$$

where θ is the direction in which the wave component is propagating (clockwise from north), ω is the angular frequency and, $\hat{\mathbf{k}} = (\sin(\theta), \cos(\theta))$ is a unit vector in the direction of the wave component. This is a costly operation to perform for all model points, and often, as in this study, the full wave spectrum is not available. Therefore, we use an approximate profile based on the parametric spectrum by Phillips (1958). Integrating over all directions, the one-dimensional frequency spectrum reads

$$F(\omega) = \int_0^{2\pi} E(\omega, \theta) \quad d\theta. \tag{23}$$

Substituting Eq. (23) in Eq. (22) and using the Phillips spectrum (Phillips, 1958), an approximate profile of the Stokes drift speed $v^s = |\mathbf{U}^s|$ can be obtained, by integrating for all frequencies (Breivik et al., 2016), in the form

$$v^s(z) = v^s(0)[e^{2\bar{k}z} - \beta\sqrt{-2\bar{k}\pi z} \ \mathrm{erfc}\,(\sqrt{-2\bar{k}z})], \tag{24}$$

where erfc is the complementary error function. The inverse depth scale can be estimated from the surface Stokes drift and the Stokes transport [see Eq. (23) by Breivik et al. (2016)], $\bar{k} = (v^s(0)/2V)(1 - 2\beta/3)$, where β is a constant, and, as suggested by Breivik et al. (2016), it is generally close to unity, which is what we assume in this study. The Stokes transport can be estimated from the mean wave frequency $\bar{f}$, the mean wave direction and the significant wave height H_{m_0}, $\mathbf{V} = (2\pi/16)\bar{f}H_{m_0}^2\hat{\mathbf{k}}_s$ (Breivik et al., 2014). However, in this study the surface Stokes drift and Stokes transport are interpolated from the WAVEWATCH III hindcast, computed directly from the full wave energy spectrum. These two parameters will be enough to reconstruct the profile (24). However, averaging over the instantaneous hybrid coordinate is required in HYCOM, therefore in order to reconstruct the layer-averaged profile, we use the integrated form of Eq. (24) that represents the Stokes transport between a level z and the surface, given in the form (Li et al., 2017)

$$V(z) = \frac{v^s(0)}{2\bar{k}} \left\{ 1 - e^{-2\bar{k}|z|} - \frac{2\beta}{3} \left[1 + \sqrt{\pi}\,(2\bar{k}|z|)^{\frac{3}{2}} \ \mathrm{erfc}\,(\sqrt{2\bar{k}|z|}) \right. \right. $$
$$\left. \left. - (1 + 2\bar{k}|z|)e^{-2\bar{k}|z|} \right] \right\} . \tag{25}$$

Thus the Stokes drift averaged on a layer with upper interface at z_{top} and lower interface at z_{bot} is estimated as

$$\langle v^s \rangle = \frac{V(z_{\mathrm{bot}}) - V(z_{\mathrm{top}})}{|z_{\mathrm{bot}}| - |z_{\mathrm{top}}|} . \tag{26}$$

where again $\beta = 1$. Using 2D parameters from the WAVEWATCH III

hindcast as input to HYCOM, i.e, the surface Stokes drift velocities and the Stokes transport, the layer-averaged profile is computed online using the depths of the pressure interfaces. The direction of Stokes drift is chosen to be in the direction of the Stokes transport and assumed to be constant with depth. The reconstructed and layer-averaged Stokes profile in HYCOM has been verified by computing its transport and comparing it against the corresponding Stokes transport from WAVE-WATCH III, a very good agreement is found. Therefore the wave momentum is conserved in the layer-averaged reconstruction.

We use the surface layer averaged Stokes drift $\langle v^s \rangle_{\mathrm{SL}}$, Eq. (26), to compute $\mathrm{La_{SL}}$. Because of the large depth of the mixed layer (here the surface boundary layer) in this study, the impact of the reference Stokes drift v^s_{ref} is negligible and is therefore taken to be zero, similar to the approach by Li et al. (2016) and Reichl et al. (2016a).

2.4. Experimental setup

The model has been initialized from a climatology of the World Ocean Atlas of 2005 (Locarnini et al., 2006; Antonov et al., 2006), and spun up for 8 years from which the first two years are forced with climatology and the rest with realistic forcing. The atmospheric forcing is interpolated from six-hourly fluxes from ERA-Interim, with grid resolution of approximately 79 km (Dee et al., 2011). The wave parameters cover the world oceans to 80°N with three-hourly temporal resolution which has been linearly interpolated at every model time step (800 s). The spatial resolution of the wave parameters is 1/2°, which is interpolated to the TOPAZ4 grid. All experiments are integrated for 3 years covering the period 2010–2012.

The comparison of the impact of the parameterized Langmuir turbulence mixing is performed using six experiments presented in Table 1, where column 2 represents the experiment name, as well as it refers to the corresponding parameterization, and the third column shows the enhancement factor (see also Fig. 1). In addition, a separate experiment (CSFSm02) is conducted where the parameterization of the LT of Smyth et al. (2002) is combined with the Coriolis-Stokes force, Stokes tracer advection and the wave-modified stress. It should be noted that the enhancement factor $\mathcal{E}(\mathrm{La}_t)$ in the case of the first four parameterizations (MS00, Sm02, Tk10) is also applied to the velocity scale w_s of the unresolved shear in shown in Eq. (9). However, this is not the case for the last two parameterization VR12 and LF17, where the unresolved shear is enhanced either by the addition of Stokes term in denominator of Ri_b or by an enhanced entrainment buoyancy flux as in Eq. (20).

To investigate the performance of the different Langmuir turbulence parameterizations on different geographical regions, we split the domain into three sub-regions as shown in Fig. 2: "Nordic" covering Nordic seas, "SubPlg" covering the Sub-polar gyre region and "SubTrp" covering the rest of the North Atlantic (south of 50°N), while the whole domain will be referred to as "WholeD".

2.5. Validation data

In order to assess the wave effects on the surface temperature, we use SST from the Operational Sea Surface Temperature and Sea Ice Analysis (OSTIA) dataset from the MetOffice (Donlon et al., 2012), representing globally interpolated data on 24-h temporal resolution. It has been obtained from the CMEMS server[1], and interpolated to the model domain (see Fig. 2 (II)).

The MLD Climatology data used here comes from de Boyer Montégut et al. (2004) updated to include Argo float data to 2012 (Rodgers et al., 2014) (gridded in 1°), its winter and summer means (interpolated to the model domain) are plotted in Fig. 2 (I). In this data set the MLD has been diagnosed using the density profile criterion,
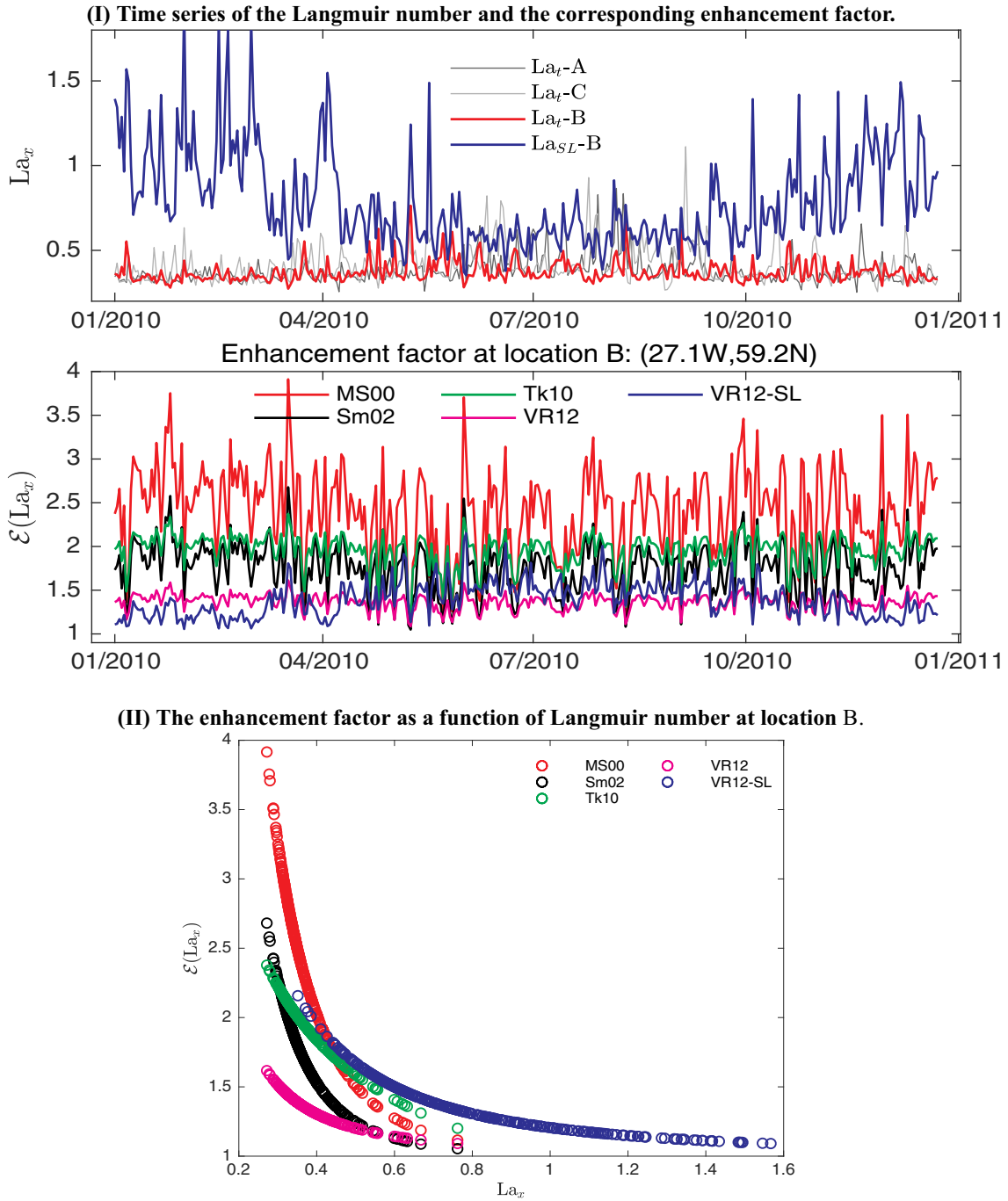
---

[1] http://marine.copernicus.eu

(I) Time series of the Langmuir number and the corresponding enhancement factor.

(II) The enhancement factor as a function of Langmuir number at location B.

Fig. 1. Panel (I) shows the daily averaged time series of (top) the Langmuir number from locations (A,B,C) (see Fig. 2) and (bottom) the corresponding enhancement factor at the test point B. Panel (II) illustrates the enhancement factor as a function of the Langmuir number. La_t-A in the legend means La_t from location *A* and so on for others, and La_x refers to La_t or La_{SL} in the case of LF17 (VR12-SL, blue line). The enhancement factors by MS00, Sm02, Tk10, VR12 and VR12-SL(or LF17) are plotted using, respectively, Eqs. (14), (15), (16), (17) and (21). Note that the enhancement factor for Sm02 (black curve) is plotted with a constant convective velocity. The MS00 enhancement factor has much higher mean and variance than the other parameterizations.

defined as the depth at which the potential density differs from its surface value by a fixed threshold of $0.03\,\mathrm{kg\,m^{-3}}$. We use the same density criterion to calculate the MLD fields from daily mean profiles, then the monthly mean MLD fields are obtained by averaging the daily mean MLD fields.

The heat content estimates are computed following Skagseth and Mork (2012),

$$\mathrm{HC} = c_p \rho_0 \int_{-H}^{0} (T - T_{\mathrm{ref}}) \ \mathrm{d}z, \tag{27}$$

where HC is the heat content, c_p the specific heat capacity of sea water, ρ_0 a reference density and H the depth. In our study, the reference temperature (T_{ref}) is zero degrees Celsius as suggested by Skagseth and Mork (2012). Heat content estimates from the model runs (monthly averages) are compared to those estimated from the monthly gridded ($1/2°$ grid) Coriolis Ocean Dataset for Reanalysis (CORA) temperature dataset (Cabanes et al., 2013). The CORA dataset is a collection of quality controlled temperature and salinity in-situ measurements collected from different sources and provided by the Coriolis data center and distributed by CMEMS (Szekely et al., 2016). The raw data received

(I) MLD mean; (left) winter and (right) summer from (a,b) climatology and (c,d) Cntl run
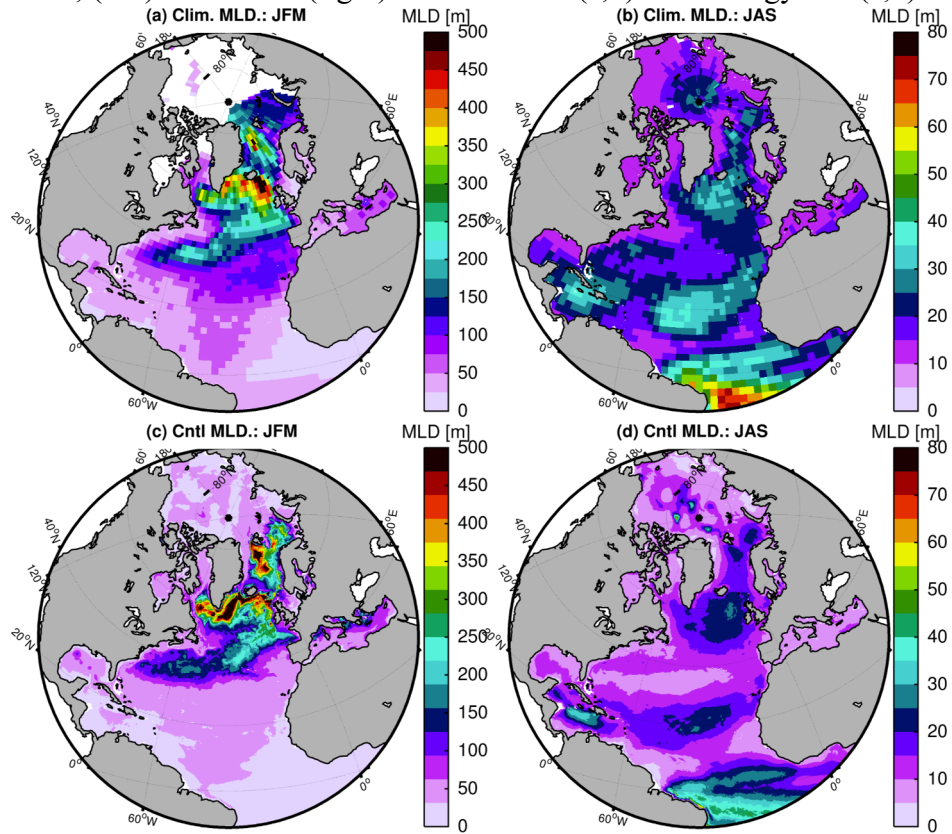
(II) SST mean; (left) winter and (right) summer from (a,b) OSTIA and (c,d) Cntl run
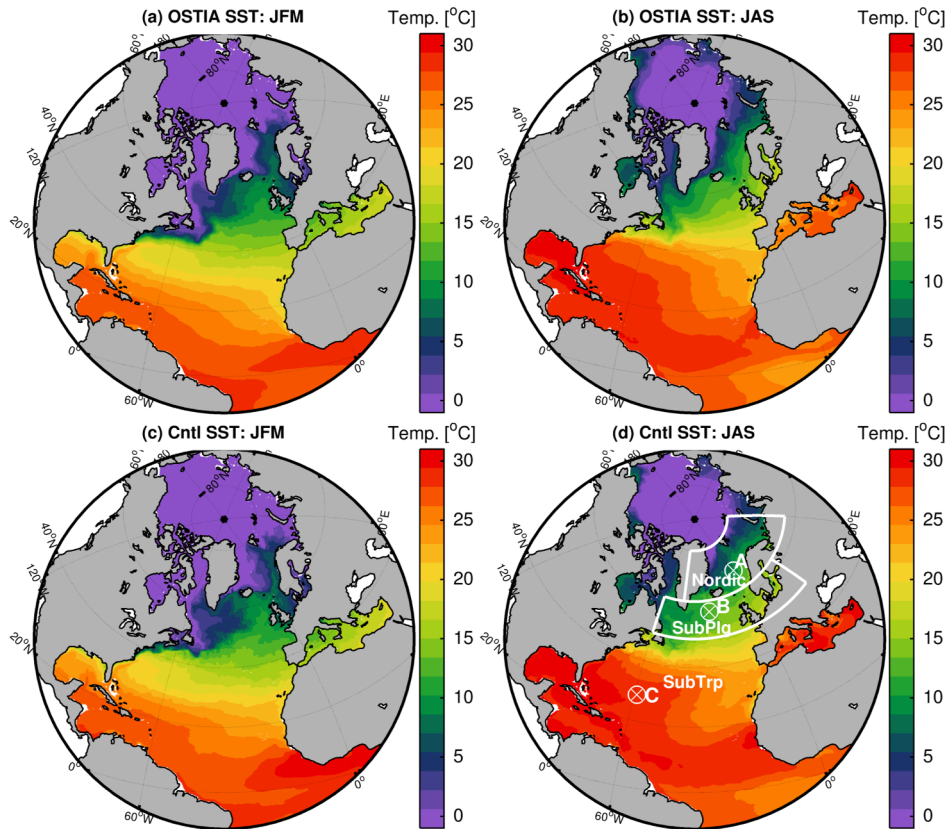
(caption on next page)

Fig. 2. Maps of (I) MLD and (II) SST from (a,b) observations and (c,d) model run with no wave effects, where (left) represents winter mean and (right) summer mean. Observations for MLD represent the climatology of de Boyer Montégut et al. (2004) updated to include Argo profiles to 2012, and for SST are from the OSTIA dataset (Donlon et al., 2012). The subregions in panel (II)d are simply denoted as Nordic, SubPlg and SubTrp, these mainly cover regions of Nordic seas, Sub-Polar gyre and Sub-Tropics (rest of the domain south of 50°N), respectively, while the whole domain is referred to as WholeD. The color scales for MLD (SST) are meter (° Celsius). The locations marked with A,B,C are used for the plot in Fig. 1.

by the Coriolis data center from different sources are put through a set of real or near-real time quality control procedures to ensure a consistent dataset (Coatanoan and de la Villeon, 2005).

To investigate the influence of Langmuir turbulence on the subsurface structure, the temperature profiles are compared with observations from the EN4 dataset (Good et al., 2013). The EN4 dataset is a large historical collection of quality controlled ocean temperature and salinity profiles. The comparison is performed by first interpolating the model daily-averaged fields horizontally to the location of the observed temperature profiles, and vertically to z-levels where the observed profiles have been sampled. The horizontal interpolation is performed using a bilinear technique. Then the interpolated daily-averaged profile is directly compared with the corresponding instantaneous EN4 profile, therefore no temporal averaging of the observations has been performed.

In this paper, the winter and summer means are computed, respectively, over January–March(JFM) and July–September(JAS), both means are from a three-year model average. All the observations of SST, MLD, heat content and temperature profiles are absolute values, not anomalies relative to a given period. This also applies to their model counterparts.

3. Simulation results

It is expected that the parameterized Langmuir turbulence enhances upper ocean mixing, potentially reducing ocean model biases in regions and seasons in which the MLD is underestimated. Here we assess the impact of LT parameterizations as well as the other wave effects described in Section 2 on the forecast model TOPAZ4. The operational version of the TOPAZ4 system[2] overestimates the winter MLD and underestimates it in spring and early summer by about 40 m. This behavior is relatively common in ocean models, (e.g., Griffies et al., 2009; Sallée et al., 2013; Williams et al., 2018). A synthesis of ocean re-analyses in the Arctic (Uotila et al., 2018) has shown that models generally overestimate deep mixing in winter and vice-versa in summer.

The forecast SST is already too cold all year round when compared to in situ buoys (by about 0.3 K) and satellite SST (by about 0.1 K), so the wave mixing is probably not the main source of error in the 28-layer configuration of TOPAZ4. In the 50-layer configuration used here (without wave effects), as will be shown, the MLD is underestimated in the rest of the domain (area south of 50°N; referred to as SubTrp) all year-round but still too deep in winter in the Nordic and sub-polar gyre (SubPlg) areas. The SST is also overestimated in subtropics in all seasons, but underestimated in winter in the areas Nordic and SubPlg. So even though some LT parameterizations should in principle degrade the solutions in the SubPlg and Nordic areas, there is room for improvement in the SubTrp region further south.

To assess the parameterizations of Langmuir turbulence in our 50-layer setup of TOPAZ4, we focus mainly on the effects on the sea surface temperature, the ocean heat content and mixed layer depth by running six experiments (see Table 1) and comparing the results against independent observations. Additionally a test is performed using the experiment CSFSm02.

Some examples of the range of the Langmuir number used here are shown by the daily mean time series at the locations (A,B,C) plotted in Fig. 1, along with the enhancement factors plotted against the Langmuir

number. As can be seen, MS00 induces the strongest enhancement factor with the highest mean and variation, followed by Tk10, Sm02, and VR12, while the La_{SL}-dependent enhancement factor (21) used in LF17 induced a seasonal variability in which the LT mixing is enhanced during summer and reduced during winter. The seasonality of the enhancement factor (21) is due to La_{SL} which, as a result of the significant difference between the summer and winter boundary layer thickness, becomes small (strong wave effects) during summer and large during winter. Fig. 1 (II) illustrates how the magnitude of enhancement factors varies when plotted against La_t, while the blue curve represents the enhancement factor (21) plotted against La_{SL}. As also seen, La_{SL} shows a larger seasonal variability than La_t.

3.1. Influence on mixed layer depth

To examine and validate the impact from each of the different parameterizations, the model MLD is compared with the climatology data of de Boyer Montégut et al. (2004), updated to include Argo data to 2012 (Rodgers et al., 2014), where the modeled MLD is diagnosed using the same density criterion as used for the climatology. The winter (JFM) and summer (JAS) means of MLD from both the climatology and model control run Cntl (with no wave effects) are plotted against each other in Fig. 2 (I).

Moreover, maps of the mean MLD bias against observation, for winter and summer averages, computed for the six experiments (Table 1) are shown in Fig. 3. This figure indicates that the MLD in the Cntl run is shallower than observations almost everywhere in summer (Fig. 3 (ii)a), whereas in winter too deep MLD can be observed around the Labrador and Nordic seas, as well as shallower MLD in the sub-tropics (Fig. 3 (i)a). Similar to the results obtained by Fan and Griffies (2014), and as shown in Fig. 3 (i)b&c, the predicted MLD is significantly degraded with the MS00 scheme in the Labrador sea region, and to a lesser extent with Sm02, (see Fig. 4 in Fan and Griffies (2014)).

The shallow MLD biases can be seen to be reduced when adding the Langmuir mixing effects as given in Fig. 3 (ii)(c,d,e,f). Notably, the parameterizations from Sm02 (Smyth et al., 2002) and Tk10 (Takaya et al., 2010), as well as VR12 (Li et al. (2016)) yield reductions in summer biases at high latitudes and in the subtropics (Figs. 3 (ii) and 4(I)). These improvements are reflected by reduced MLD root-mean-square errors (RMSE) as shown Fig. 5 (I)). In winter, however, the parameterized LT effects appear to introduce too strong mixing, as a consequence, the MLD prediction in the Labrador and Nordic seas is degraded. In addition, many shallow biases become deep biases, in particular when using the MS00 scaling (Fig. 3 (i)b).

The percentage increase on MLD due to LT mixing is shown in Fig. 6. The distribution of the zonal-mean MLD bias given in Fig. 4 (I) (computed from Fig. 3) shows that the LT parameterizations by MS00, Sm02, Tk10 and VR12 exhibit a strong MLD deepening during winter at high latitudes, and hence the RMSEs are increased as shown in Fig. 5 (I). These results may not be surprising as these four LT parameterizations are based on La_t and generally give the strongest enhancement as shown in the middle panel in Fig. 1. As seen from this figure, the La_{SL}-based enhancement factor (21) has lower values during winter.

On the contrary, the LF17 scheme, which adds the enhanced entrainment buoyancy flux and adopts the surface layer averaged Langmuir number La_{SL}, appears to be the only scheme which introduces stronger MLD deepening in summer than in winter (see Fig. 6), and therefore leading to improvements on MLD during both summer winter

---

[2] See http://marine.copernicus.eu and the validation report therein.

(i) Winter mean

(ii) Summer mean

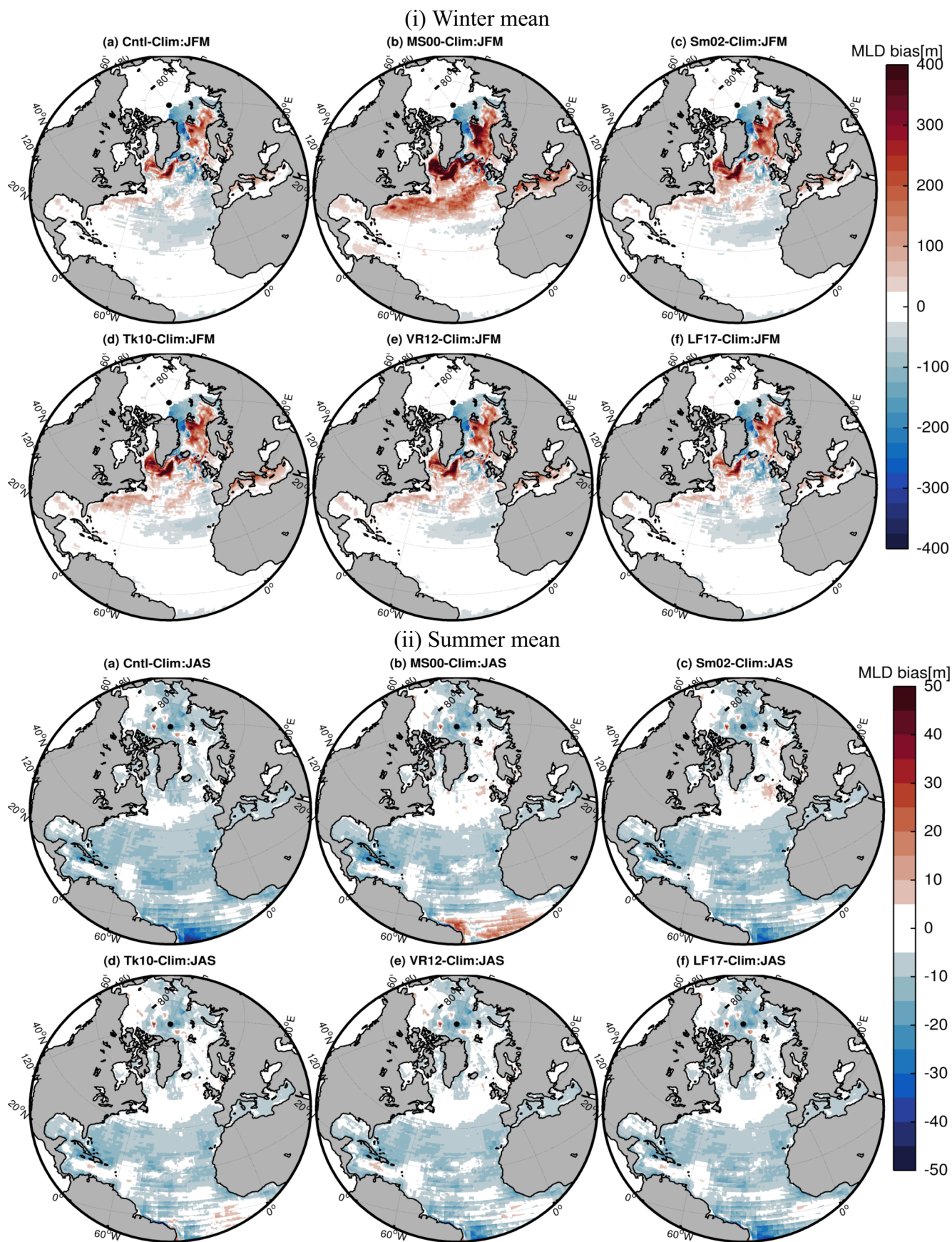**Fig. 3.** Maps of the bias in the (i) winter and (ii) summer mean mixed layer depth against climatology of de Boyer Montégut et al. (2004) updated to include Argo data to 2012. The bias is computed as (Model MLD - Clim MLD) for the experiments (a) Cntl (without wave effects), (b) MS00 (McWilliams and Sullivan, 2000), (c) Sm02 (Smyth et al., 2002), (d) Tk10 (Takaya et al., 2010), (e) VR12 (Van Roekel et al., 2012) and (f) LF17 (Li and Fox-Kemper, 2017).
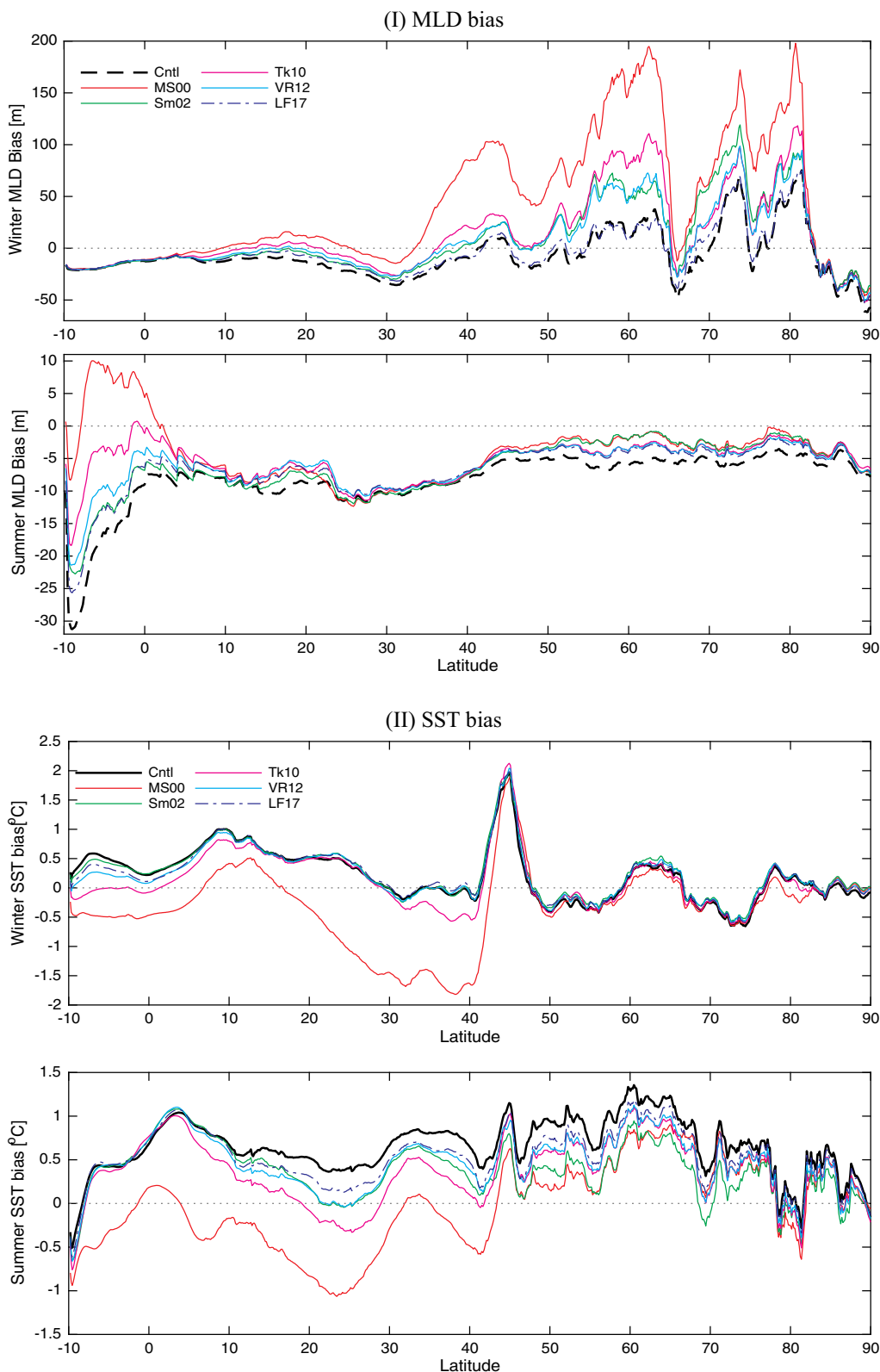
Fig. 4. Zonal means of (I) MLD bias computed from Fig. 3, and (II) SST bias computed from Fig. 8. For each (I)&(II), (top panel) represents winter mean and (bottom panel) is the summer mean. The subregions SubTrp, SubPlg and Nordic are, respectively, located within (south of 50°N), (50°N-63°N) and (63°N-80°N).

without exaggerating the existing deep biases (Fig. 5 (I)).

In winter, as the MLD is already deep at high latitudes, small improvements are generally south of 50°N (Figs. 4 (I) and 5(I)). Interestingly, with the LF17 scheme a weak shallowing between 50 and 70° N (region of strong convection) appears during winter, see Figs. 4 (I) and

5(I). This is probably due to shallowing by the modified unresolved shear velocity (20) under strong convective conditions. Fig. 4 (I) displays large summer negative MLD biases between latitudes 3° S and 10° S, which can be related to the southern hemisphere winter where the MLD deepening increases as shown by the observation in Fig. 2 (I)b
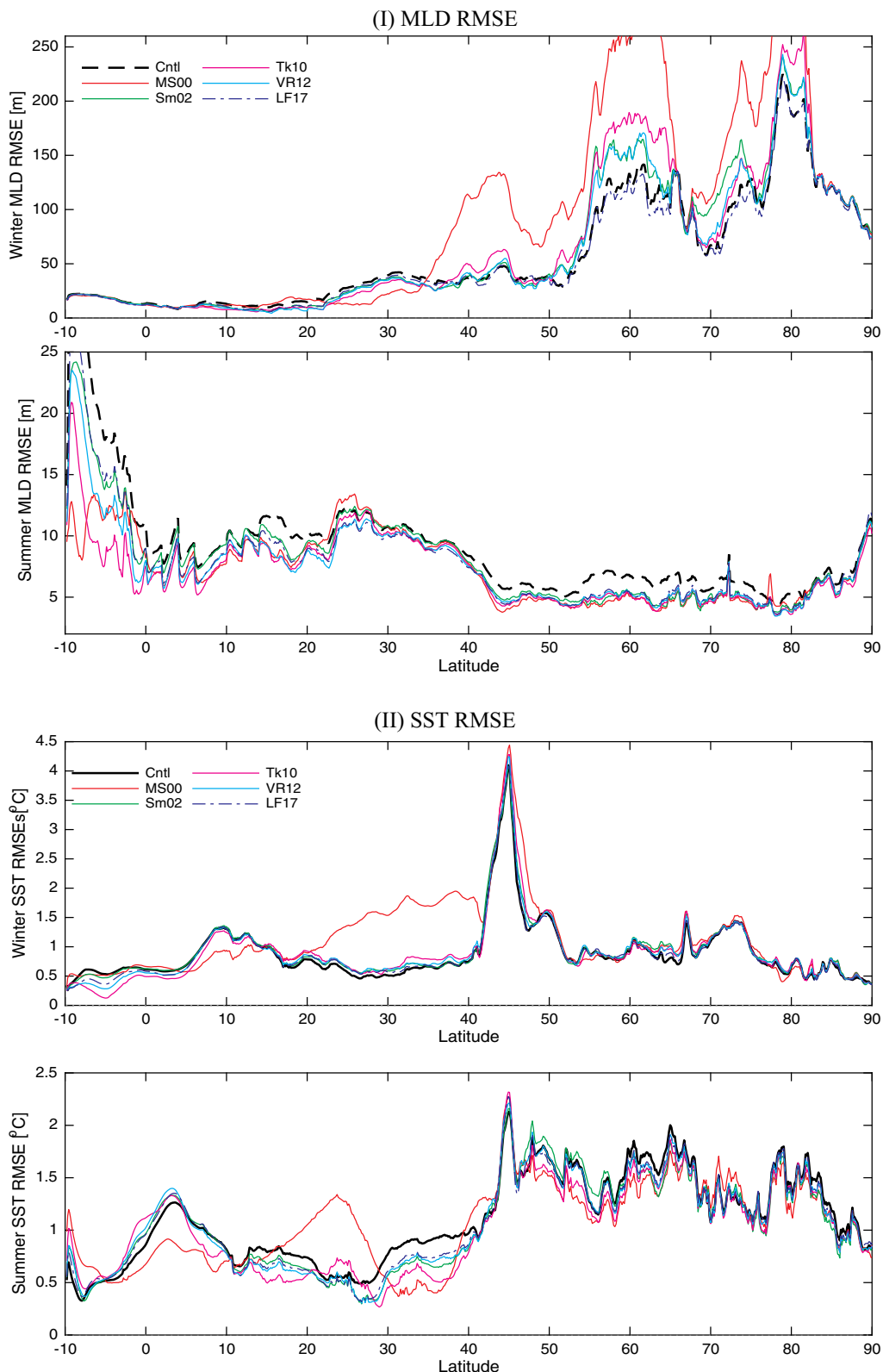
Fig. 5. Same as Fig. 4, but here it shows the zonal mean of RMSE of (I) MLD and (II) SST. Note that there appear slight reductions in MLD RMSE north of 50 N during winter with LF17 approach.

but not well captured in the Cntl run (Fig. 2 (I)d). The model is relaxed to the climatology at the southern open boundary, so the difference between this climatology and MLD observations (see Fig. 2) could also contribute to these errors. Adding that the Langmuir mixing effect appears to slightly reduce these negative biases.

The performance of Langmuir mixing parameterizations varies depending on regions and regimes. All the parameterizations considered in this study tend to deepen the MLD compared to the control run (Table 2). Except with the LF17 approach, the impact in winter is clearly much stronger than in summer (Fig. 6). In particular the
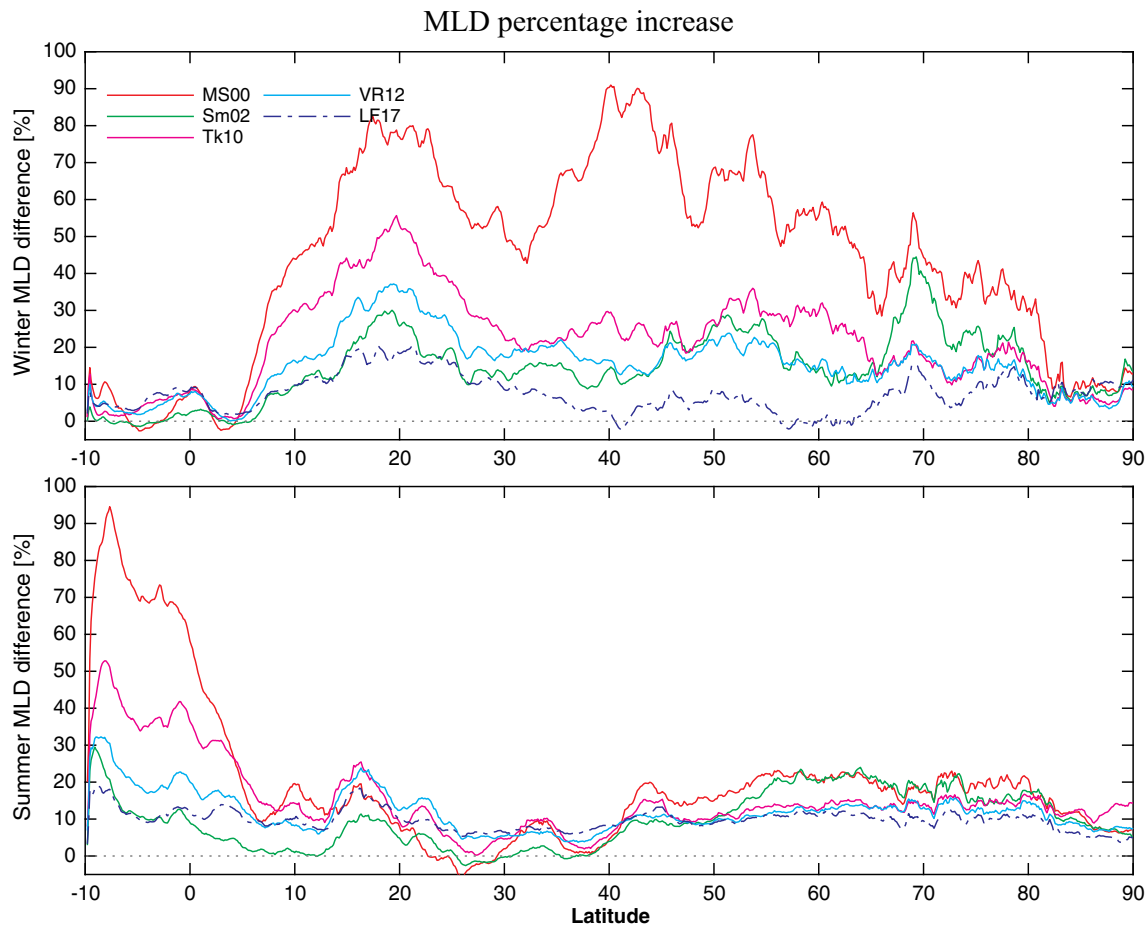
Fig. 6. Zonal mean of the percentage increase (%) on MLD relative to the control run Cntl in (top) winter and (bottom) summer averaged over three years, showing how significant the impact of the Langmuir mixing induced by (a) MS00, (b) Sm02, (c) Tk10, (d) VR12 and (f) LF17 parameterizations. The subregions SubTrp, SubPlg and Nordic are, respectively, located within (south of 50°N), (50°N-63°N) and (63°N-80°N).

Table 2
Mean percentage increase (%) in MLD when including the Langmuir mixing relative to the control run (Cntl) with no wave effects. The subregions Nordic, SubPlg and SubTrp are depicted in Fig. 2 (ii), and WholeD refers to the whole model domain.

Scaling	Winter (JFM)				Summer (JAS)			
	Nordic	SubPlg	SubTrp	WholeD	Nordic	SubPlg	SubTrp	WholeD
MS00	37.7	49.5	53.3	42.8	20.7	27.8	14.6	20.8
Sm02	27.4	22.3	12.6	13.6	19.1	28.9	4.2	8.8
Tk10	17.6	23.2	26.7	21.6	15.2	16.8	13.8	16.4
VR12	16.6	17.4	17.7	15.2	13.3	16.9	10.5	13.0
LF17	8.3	3.8	8.2	8.2	11.2	14.5	9.4	9.8

parameterization by MS00 induces too vigorous mixing which leads to excessive MLD increase in the winter over large regions.

Table 2 presents the MLD percentage increase averaged over the whole region and the three subregions (see Fig. 2), and for both winter and summer means (from three-year average). This illustrates again that there is a clear seasonality of the influence of the Langmuir mixing where deepening in winter is more pronounced, for instance, when averaged over the whole domain. However, this is not the case for LF17 parameterization for which the percentage increase in MLD during summer is larger than during winter.

The percentage increase on MLD induced by the parameterization of LF17 at high latitude (Fig. 6) appears to be roughly close to the ranges (15–20 %) shown by D'Asaro et al. (2014), who used a completely different turbulence model than KPP to account for the Langmuir mixing.

It should be observed that (in Table 2) the mean percentage MLD deepening due to the MS00 scheme in winter on region SubPlg is more than double that induced by Sm02 (Smyth et al., 2002), while both MS00 and Sm02 parameterizations induce approximately an equivalent percentage deepening on this region in summer (Fig. 6). This is due to the inclusion of the stability effects in Sm02 scaling which works to suppress the MLD deepening under convective conditions which are favorable during winter over region SubPlg. However still the winter MLD is exaggerated with Sm02 in this region (Fig. 4 (I)). The excessive mixing induced by the MS00 and Sm02 scalings agrees with findings by Li et al. (2016) when adopting the same schemes in the CESM with POP2.

Instead of applying a single enhancement factor for both the unresolved shear and the eddy viscosity, the VR12 and LF17 use a separate enhancement for the unresolved shear as shown in Table 1. The high
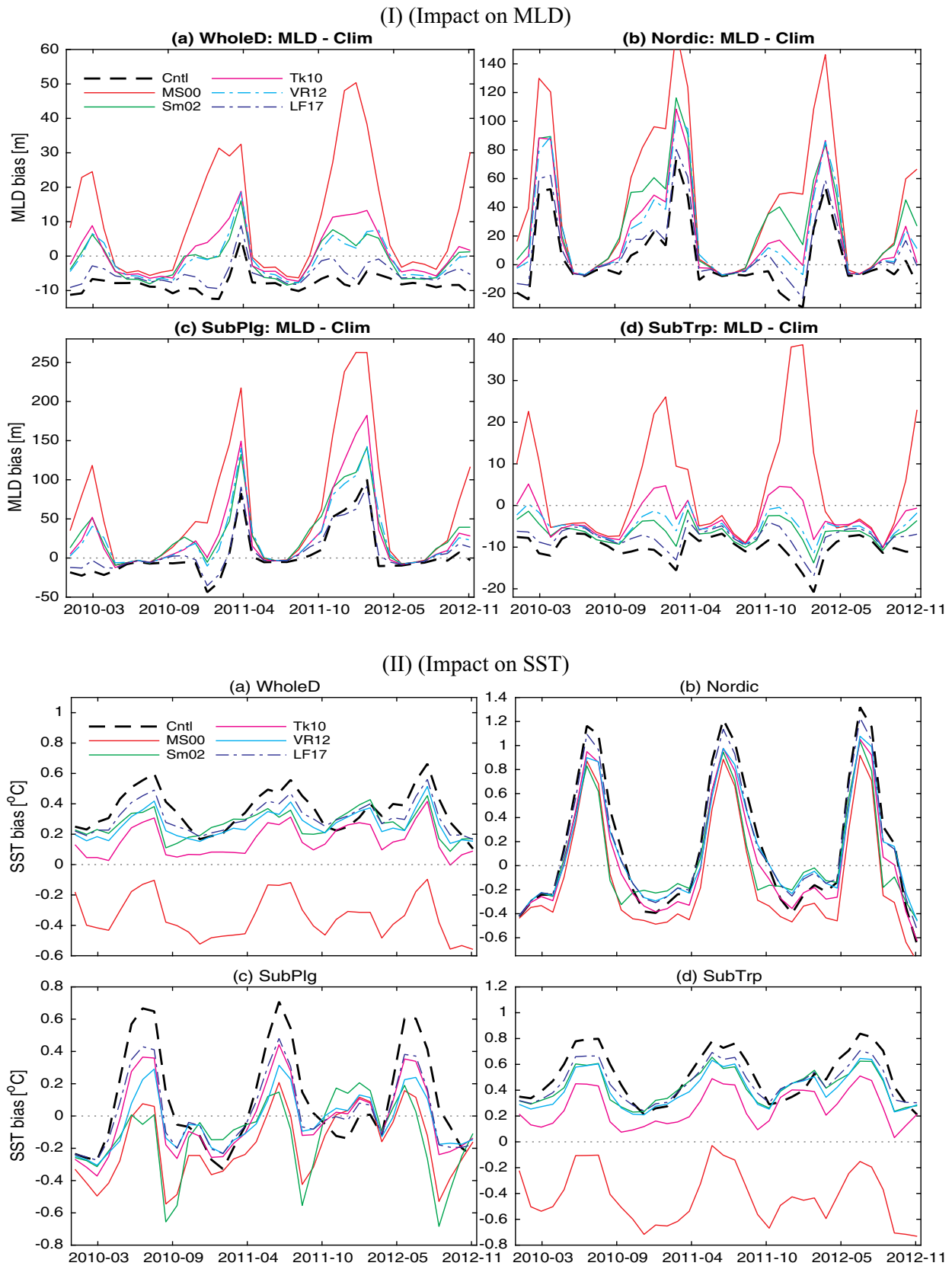
Fig. 7. Time series of the mean (I) MLD bias against climatology or (Model - climatology) (II) SST bias against OSTIA SST computed from the daily-averaged data, where the bias is spatially-averaged over the (a) whole domain WholeD, and the subregions (b) Nordic, (c) SubPlg and (d) SubTrp.

percentage increase in winter MLD with VR12 presented in Fig. 6 suggests that enhancing the unresolved shear by adding the Stokes drift term would overestimate the MLD. The consideration of the Langmuir mixing effects on the entrainment buoyancy flux by LF17 scheme (Li and Fox-Kemper, 2017) is found to restrain the excessive winter deepening (Fig. 6) and therefore appears to be a more adequate approach for enhancing the unresolved turbulent shear. Our results agree with the findings by Li and Fox-Kemper (2017) who showed that their scheme increases the MLD deepening in the southern ocean during summer while yielding only a modest impact under strongly convective winter conditions.

The temporal variability of the mean bias is also analyzed. As can be seen from the mean bias time series (Fig. 7 (I)), the MLD from the control run (Cntl, black-dash line) is always shallower than MLD from climatology data in summer, and in all seasons in the subtropics (Fig. 7 (I)d). Nevertheless, this shallow bias is significantly decreased when adding Langmuir turbulence mixing, with the LF17 parameterization yielding the best overall performance (Fig. 7 (I)a), especially during winter. In contrast, all four schemes involving the original La_t number (MS00, Sm02, Tk10, VR12) cause excessive winter-time deepening of the MLD averaged over the model domain.

3.2. Influence on ocean temperature

The Langmuir turbulence enhances upper-ocean mixing leading to deepening of the MLD, and therefore has important effects on the ocean temperature. To examine such effects on SST, model results are compared against SST observations from OSTIA. The winter (JFM) and summer (JAS) means of SST from both OSTIA and Cntl run are plotted against each other in Fig. 2 (II). The latitudinal distribution of the zonal-mean SST bias (Fig. 4 (II)) shows that adding Langmuir mixing substantially reduces warm SST biases, most notably in the summer. This is also reflected by the RMSE shown in Fig. 5 (II), which displays no noticeable RMSE reduction in winter.

The temporal variability of the mean SST bias is presented in Fig. 7 (II), which indicates that the averaged SST from the control run Cntl (dash-black line) is generally warmer than OSTIA SST, except for the winter SST in the Nordic and SubPlg areas. This can be seen more clearly in the SST error maps given in Figs. 8a. Overall, this warm bias is reduced when including the Langmuir mixing effects with the five LT parameterizations. In particular, the Tk10 scaling appears to significantly reduce the mean warm bias over region SubTrp (Fig. 7 (II)(d), purple line), however, the induced mixing appears to be too vigorous causing underestimated SST in the SubTrp region as presented in Fig. 8 (ii)d.

In region SubPlg, the VR12 scaling outperforms others in correcting both negative and positive mean SST biases (Fig. 7 (II)c, cyan line), while LF17 (Li and Fox-Kemper, 2017) parameterization introduces a bias reduction approximately similar to that induced by TK10 scaling (Fig. 7 (II)c, red-dash and purple lines). The MS00 parameterization induces too large cold SST biases south of 50°N, both in winter and summer (Fig. 4 (II), red line), also shown by the mean bias map given in Figs. 8b. Overall, the LF17 yields good reductions in the warm SST biases without causing aggressive increase in the cold biases, for example see the bias in region SubTrp in (Fig. 8 (ii)f).

During winter, the control run shows large positive SST bias, especially around the Gulf Stream, Labrador Current and in the south east Atlantic, and negative biases in the middle North Atlantic (Fig. 8 (i)a). The exception is the MS00 scaling which mixes excessively, the other four parameterizations appear to lead to only a small impact on these biases. Such biases are often related to the large-scale circulation features of the model, and the mixing parameterizations cannot directly improve their representations.

Fig. 9 shows the time series of the mean ocean heat content (down to 700 m depth) from experiments Cntl (with no wave effects) and the five Langmuir mixing parameterizations, in addition the heat content

from CORA observation (Cabanes et al., 2013) plotted in dash-gray line. A distinct seasonal cycle is depicted in the heat content of the ocean with maximum in summer and minimum in winter. In general, the heat content derived from the control run is lower than those estimated from observations (Fig. 9, dash-black line). The LT parameterizations enhance the mixing of surface water with that in the interior layers mainly, leading to a cooling of SST, and therefore indirectly increases the air-to-ocean heat flux that elevates the ocean heat uptake. From the beginning of the simulation, the ocean heat content starts gradually to increase when adding LT effects relative to the control experiment Cntl (Fig. 9), and appears to become more closer to the CORA observations. However the increase in the heat content introduced by MS00 as well as Tk10 parameterizations is too high, which is due to the strong enhancement factors associated with the two schemes as shown in Fig. 1. It is likely that this rapid increase in the heat content could have continued in ever longer simulations.
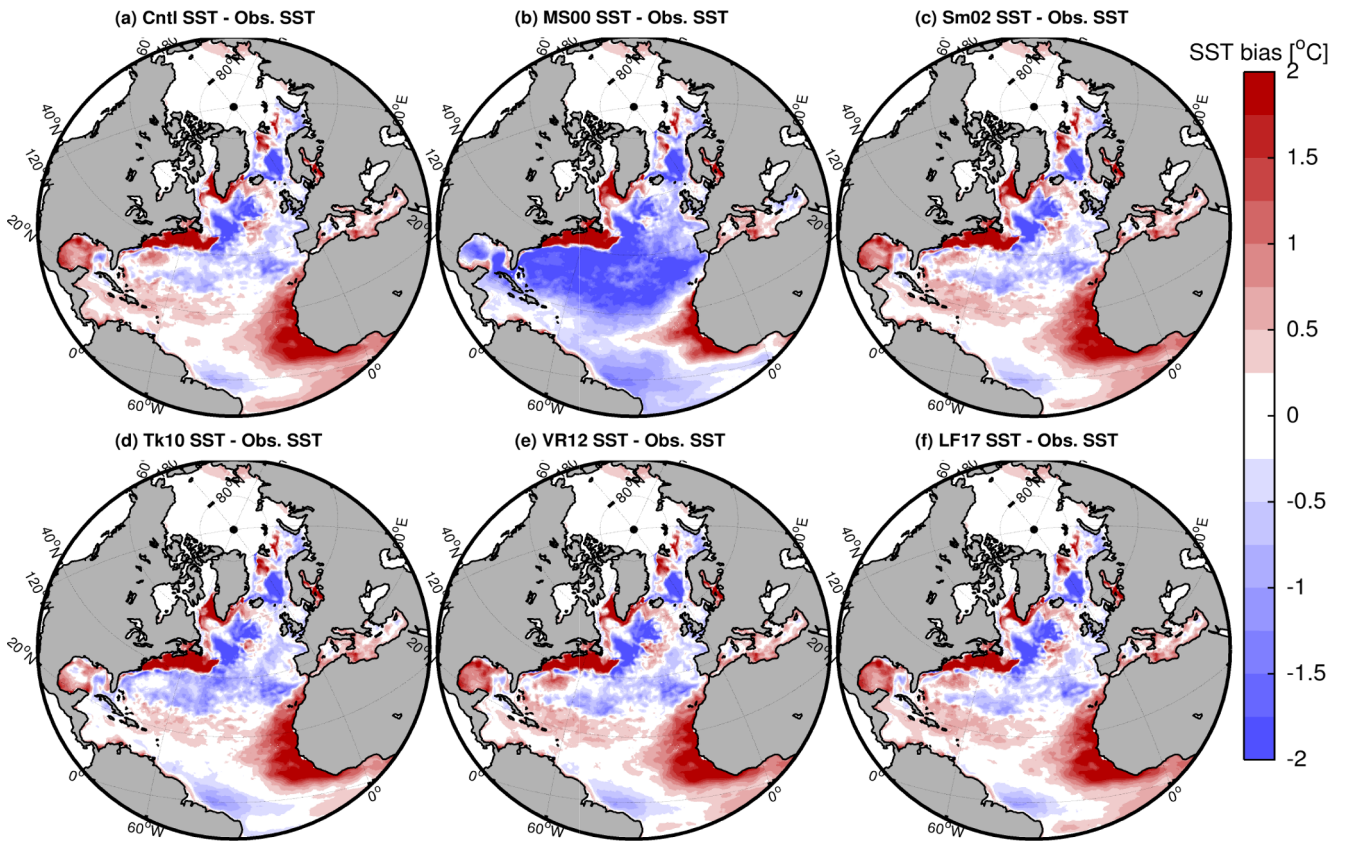
The enhancement factor by MS00 causes vigorous mixing and with it a significant injection of heat into the deeper layers. Conversely, it appears that MS00 reduces the heat content excessively on the Nordic region relative to the Cntl run (Fig. 9b, red line). Contrarily to the Subtropical regions, the Nordic Seas experience a year-round influx of warm water which lies underneath relatively cold surface water. When more mixing brings it to the surface, it can be cooled through heat loss to the atmosphere.

This heat loss in the Nordic region can be explained by the large increase in the cold bias in the temperature profiles by MS00 shown in Fig. 10 (top panels). It should be noted that there may exist an offset between the heat content in the control case and the CORA dataset, as seen for example in region SubTrp (Fig. 9d). The comparison to the time series of CORA observations yields that the phase of the seasonal cycle is late in the Cntl run, particularly in the Nordic and SubTrp regions, though the SubPlg region seems to vary in phase (Fig. 9). None of the different Langmuir mixing parameterizations does seem to change the phase of the seasonal cycle, indicating that the cause of the delays must be elsewhere.
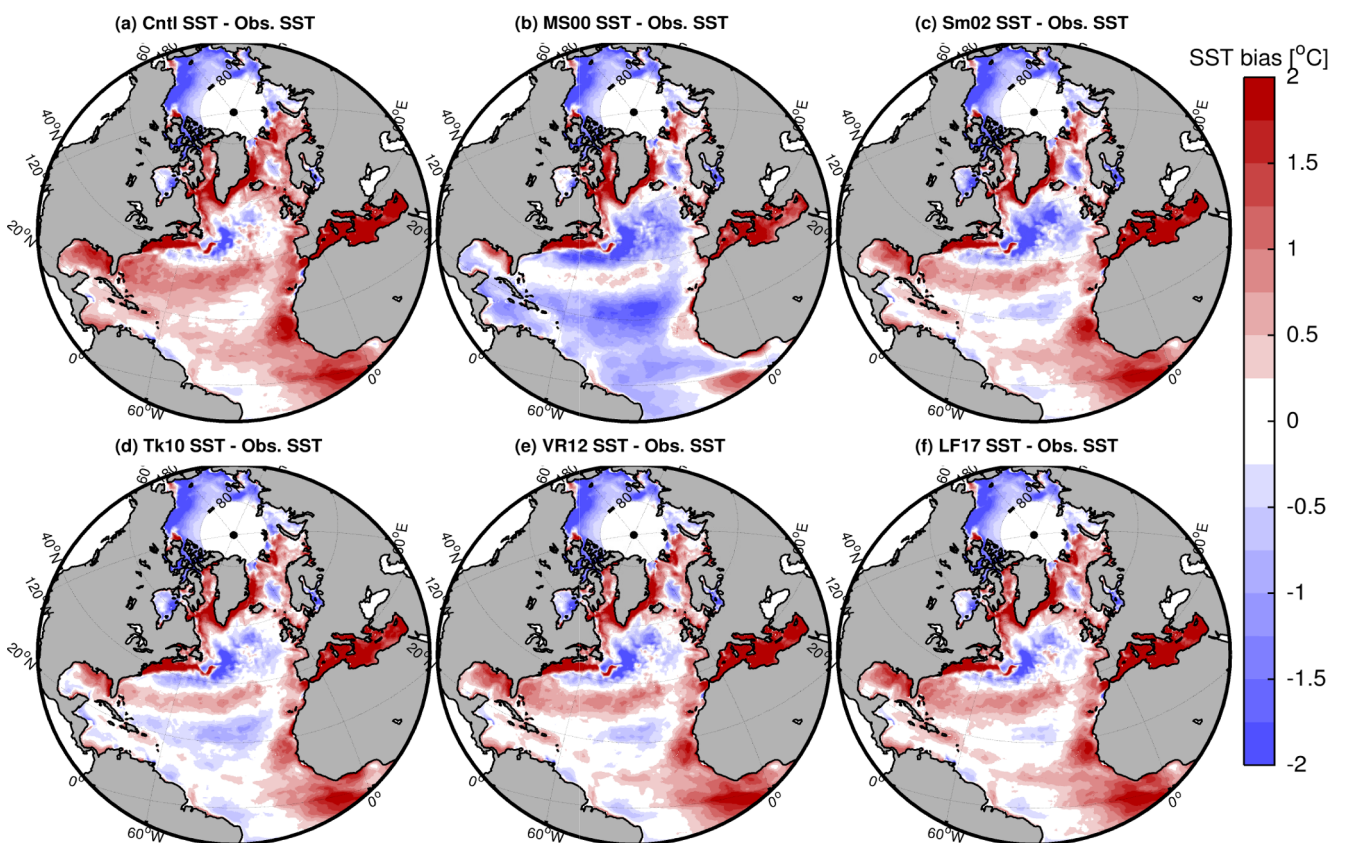
The change in the ocean heat content due to Langmuir-induced mixing indicates a change in the subsurface temperature profile. Fig. 10 shows that the different parameterizations generally tend to reduce the biases at the surface, but not necessarily the biases at all depths. Other than the winter in region SubPlg, the profiles mainly show warm near surface biases. An explanation for improvement here can be due to the characteristics of LT effects which mainly induce cooling of surface layer, and hence warm near surface biases are reduced. Only in the SubPlg region do the cold biases reduce at all depths, both in summer and winter. Elsewhere, the sub-surface biases rather seem exacerbated by the Langmuir parameterizations, even in the SubTrp region where improvements were expected due to the too shallow MLD and warm SST biases. In the SubTrp, the strong LT enhancement will cool the SST by mixing warm surface water with relatively cold subsurface water, and therefore contribute to warming the interior and to exacerbate existing warm biases.

The impact due to other wave effects is examined in experiment CSFSm02. As shown by the latitudinal distribution of the zonal-mean bias plotted in Fig. 11 (II), adding the Coriolis-Stokes force, Stokes tracer advection and the wave-dependent wind stress combined with the Langmuir mixing enhancement by Sm02 in experiment CSFSm02 introduces no noticeable differences in SST biases. Similar results are also found when computing the MLD biases (Fig. 11 (I)), suggesting that Langmuir mixing is much more important than these wave processes. This agrees with the results by Reichl et al. (2016a) who found, under idealized hurricane conditions, that the Langmuir turbulence has a much greater influence than the Coriolis-Stokes force. We have also rerun the same experiment (CSFSm02) by including the vortex force in the horizontal momentum (ignoring the wave-induced pressure), however we did not find any apparent differences. The terms involving the vorticity times Stokes drift velocities may have smaller impact than

(i) Winter mean (JFM): Model SST - OSTIA SST

(a) Cntl SST - Obs. SST (b) MS00 SST - Obs. SST (c) Sm02 SST - Obs. SST

(d) Tk10 SST - Obs. SST (e) VR12 SST - Obs. SST (f) LF17 SST - Obs. SST

(ii) Summer mean (JAS): Model SST - OSTIA SST

(a) Cntl SST - Obs. SST (b) MS00 SST - Obs. SST (c) Sm02 SST - Obs. SST

(d) Tk10 SST - Obs. SST (e) VR12 SST - Obs. SST (f) LF17 SST - Obs. SST

(caption on next page)

Fig. 8. Maps of the model SST bias against OSTIA re-analysis, computed as Model SST - OSTIA SST for (i) winter (JFM) and (ii) summer (JAS) means. The figures in (I) and (II) represent biases computed from the (a) Cntl run, and the runs with Langmuir mixing of (b) MS00 (McWilliams and Sullivan, 2000), (c) Sm02 (Smyth et al., 2002), (d) Tk10 (Takaya et al., 2010), (e) VR12 (Van Roekel et al., 2012) and (f) LF17 (Li and Fox-Kemper, 2017).

the Coriolis-Stokes force on the basis of the scale of the horizontal grid resolution used in this study, and therefore could be one reason for such negligible effects.

4. Discussion and concluding remarks

In this study, five different parameterizations (Table 1) of Langmuir turbulence mixing in the North Atlantic have been investigated using HYCOM and wave forcings from a WAVEWATCH III global hindcast (Rascle et al., 2008; Rascle and Ardhuin, 2013). These parameterizations are proposed to enhance the turbulent vertical kinetic energy, and hence the mixing in the ocean surface boundary layer through modification of the KPP scheme of Large et al. (1994). The impact due to the Coriolis-Stokes force, Stokes tracer advection and wave-modified stress in combination with the Langmuir effects have been assessed. The estimation of the Stokes drift profile based on the Phillips spectrum from Breivik et al. (2016) has now been implemented in HYCOM. The Langmuir turbulence parameterization on the boundary layer entrainment by Li et al. (2016) as well as the enhanced entrainment buoyancy flux by Li and Fox-Kemper (2017) have now been implemented in the KPP scheme used in HYCOM.

We adopted the definition of the Langmuir turbulence number following McWilliams et al. (1997), as a measure of the relative impact of the wind-driven shear to the magnitude of the Stokes drift at the surface. In addition, we have also implemented and used the surface layer averaged Langmuir number (Harcourt and D'Asaro, 2008) in the scheme by Li and Fox-Kemper (2017). Evaluation of the model results were made by comparison with climatologies of the mixed layer and ocean temperature.

It is found that the parameterized Langmuir turbulence has a rapid and significant effect on the mixed layer depth, sea surface temperature

and ocean heat content. In addition the impact is overall much stronger in winter compared to summer, except for the parameterization that uses the enhanced entrainment buoyancy flux and the surface layer averaged Langmuir number, (Li and Fox-Kemper, 2017). In contrast, the inclusion of the Coriolis-Stokes force, Stokes drift tracer advection and the wave-dependent wind stress did not introduce noticeable differences in the model results (Fig. 11).

The main improvements of our simulations when adding the Langmuir mixing are exhibited with the parameterizations by Smyth et al. (2002), Van Roekel et al. (2012) and Li and Fox-Kemper (2017), specifically in regions and season of underpredicted MLD and overpredicted SST. However, the winter MLD is strongly degraded with the schemes by Smyth et al. (2002) and Van Roekel et al. (2012), which is shown by increased RMSEs (Fig. 5). This is not the case with the parameterization by Li and Fox-Kemper (2017) which reduces the RMSE in summer while preforms as good as the control run (with no wave effects) in winter.

The scaling by Takaya et al. (2010) is found to introduce substantial improvements on SST and MLD in the subtropical region (SubTrp), especially during summer; however it appears that the induced mixing is too vigorous, which causes excessive warming of deep ocean layers and lead to a rapid increase in ocean heat content (Figs. 9 and 10, purple line). This could likely shift the model to an unstable state in longer model runs. This strong mixing with the Takaya et al. (2010) scheme, which is based on a VKE scaling by Grant and Belcher (2009), can be due to that Takaya et al. (2010) did not design and test their enhancement factor for the KPP, it was only suggested to improve the prediction of a Skin SST model during day time.

The parameterization by McWilliams and Sullivan (2000) is found to introduce the most vigorous mixing, which strongly degrades the MLD on high latitude areas during winter, whereas in summer large
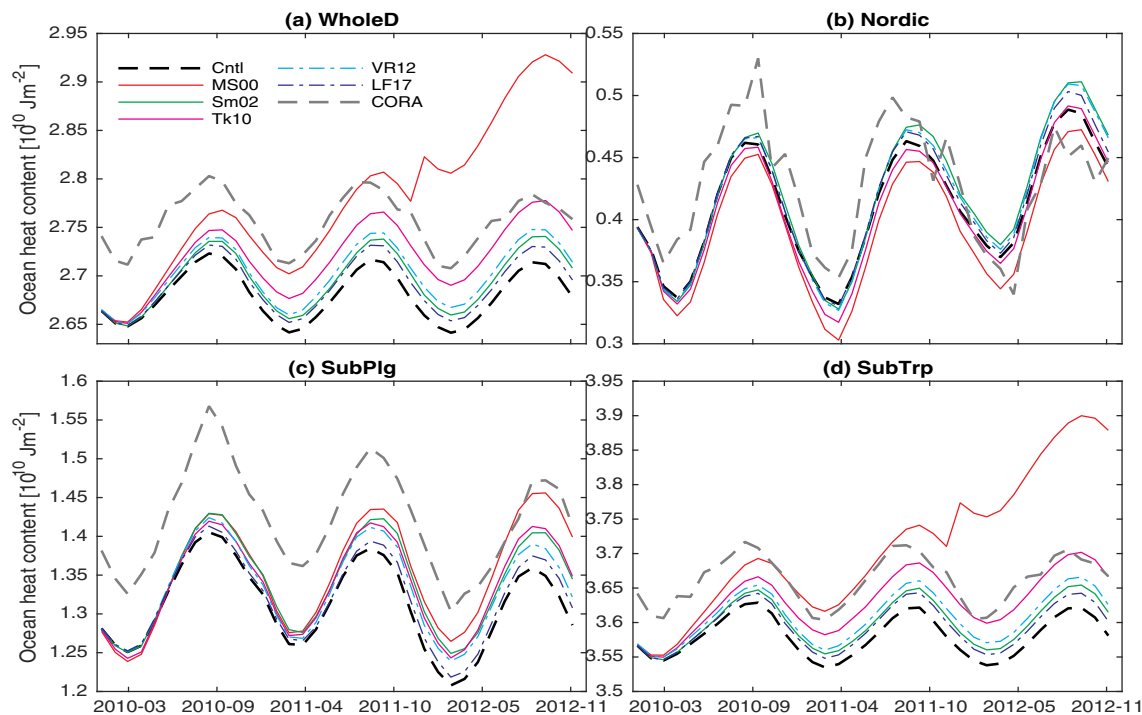

Fig. 9. Monthly time series of the heat content [10^{10} J m^{-2}] from CORA observation (dash-gray line), the control run without Langmuir mixing (dash-black line) and the five runs with Langmuir parameterizations, computed for the whole domain (a) WholeD and the subregions (b) Nordic, (c) SubPlg and (d) SubTrp. The heat content is calculated within 700 m depth.
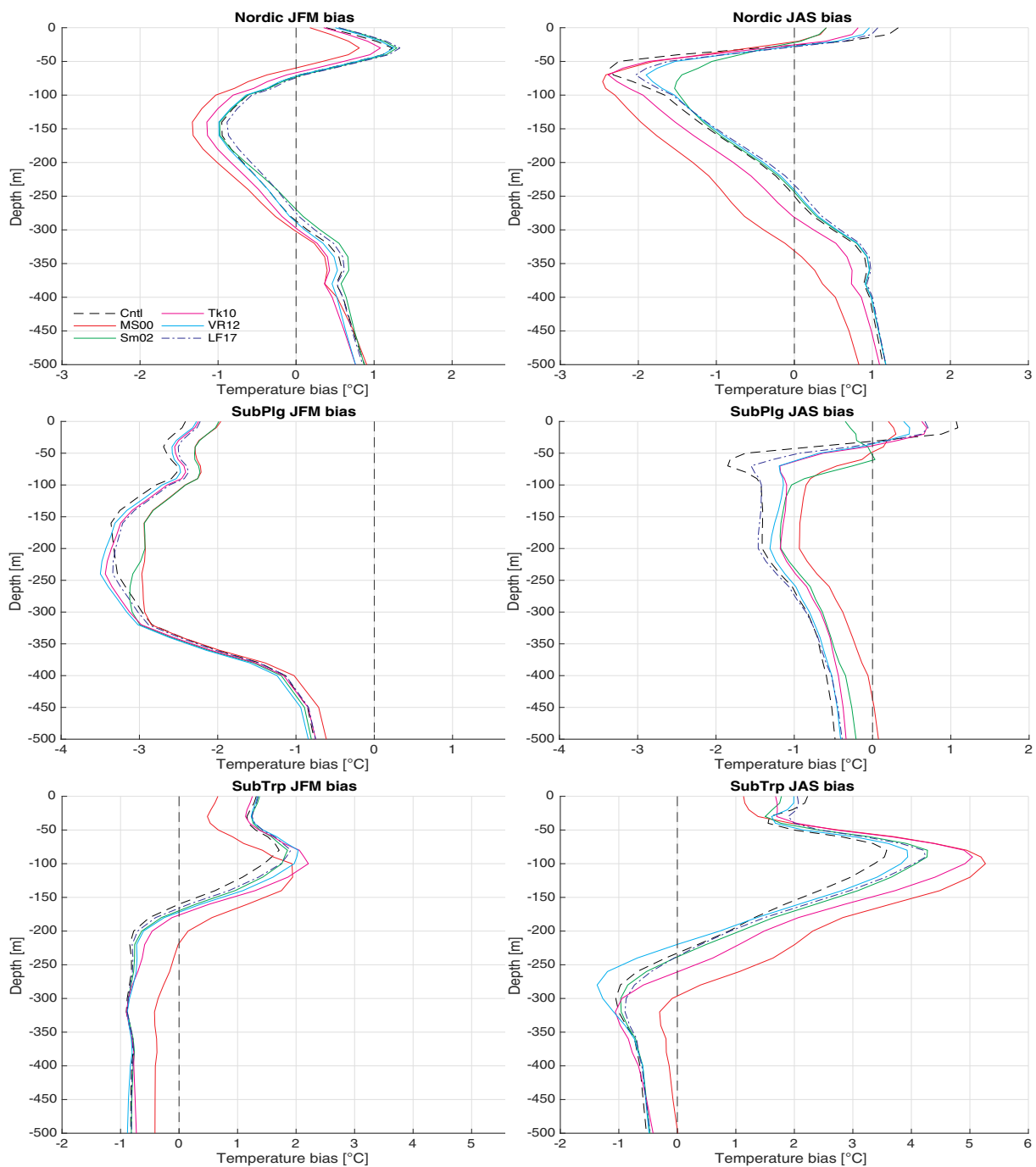
Fig. 10. Mean biases in temperature profiles against observed temperature from En4 data set (Good et al., 2013), computed for the subregions, (top) Nordic, (middle) SubPlg and (bottom) SubTrp, where (left) is winter mean and (right) summer mean. The bias is computed for the five LT mixing schemes (MS00, Sm02, Tk10, VR12 and LF17) and the control run (Cntl, black-dash line).

biases are found around the equator (Fig. 4). The scaling by McWilliams and Sullivan (2000) is shown to cool the SST excessively and to warm the deeper layers, leading to a severely exaggerated ocean heat content. In particular, the abnormal increase in the ocean heat content introduced by the scheme by McWilliams and Sullivan (2000) (Fig. 9a, red line), if continued, would shift the model into a new climate state which is clearly unrealistic. In the Nordic region, on the contrary, we find a reduction of the heat content under the scaling by McWilliams and Sullivan (2000) because the enhanced mixing exposes deep warm waters to the surface and thereby increases the heat loss to the atmosphere. Smyth et al. (2002) extended the MS00 scheme to include stability effects to restrain the excessive mixing in destabilizing/

convective conditions. Fig. 6 shows that the vigorous MLD deepening induced by McWilliams and Sullivan (2000) scheme in winter is reduced with scheme by Smyth et al. (2002), however this also true for the other parameterizations.

Overall, there is a reduction of the summertime warm SST bias when adding Langmuir mixing effects, most pronounced in the subtropical region. However, with the scalings by McWilliams and Sullivan (2000) and Takaya et al. (2010), the SST cooling is too strong which leads to an excessive and rapid warming of the ocean interior (Fig. 10). The schemes by Van Roekel et al. (2012) and Li and Fox-Kemper (2017) preform best in improving SST without increasing their RMSEs. The ocean heat content in the control run (Cntl) is found to be generally
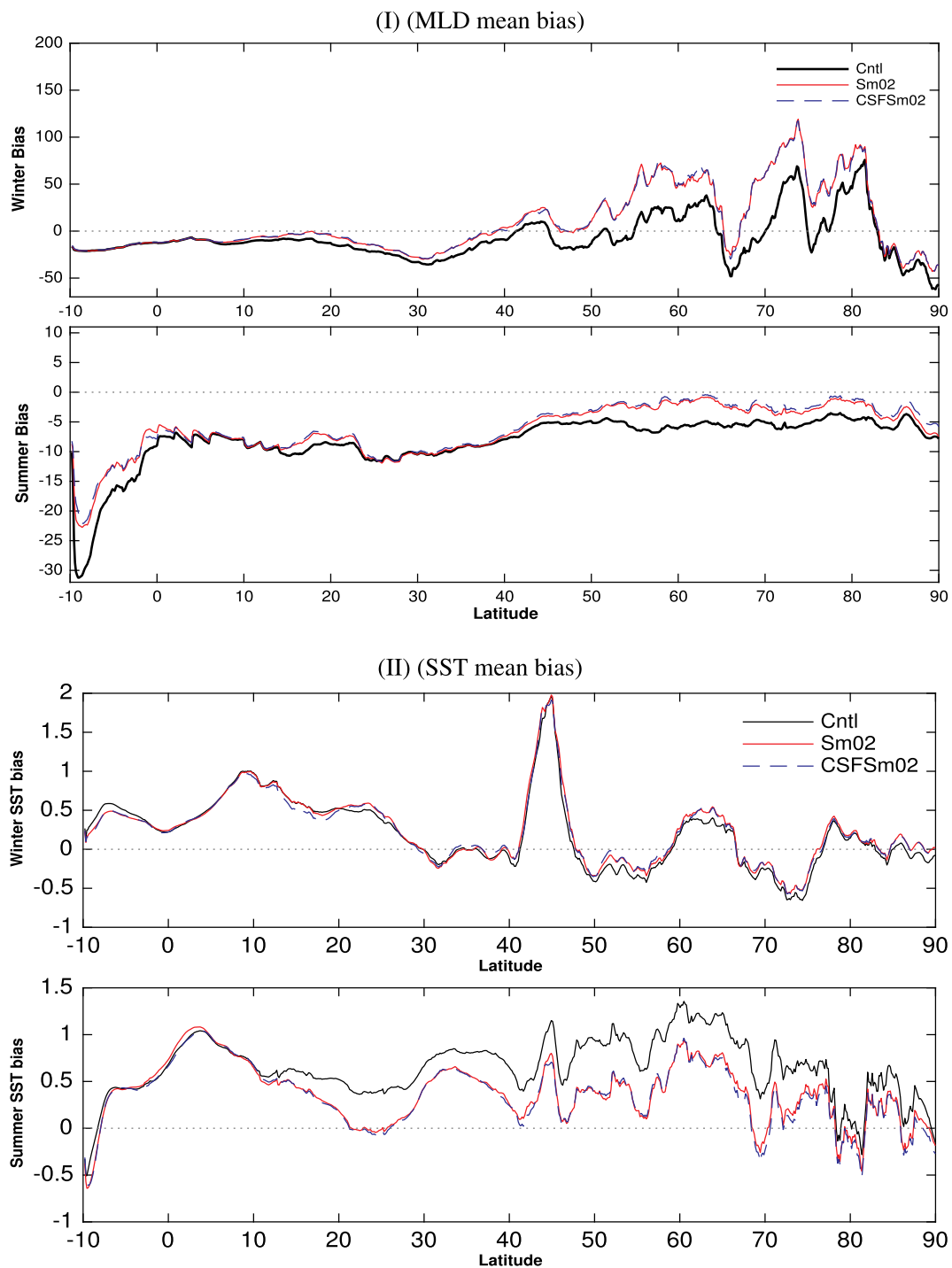
(I) (MLD mean bias)

(II) (SST mean bias)

Fig. 11. Impact of the Coriolis-Stokes force and wave dependent wind stress on (I) SST and (II) MLD. The zonal average of the bias of the control run (Cntl, black line), the Smyth et al. (2002) Langmuir turbulence parameterization(Sm02, red line) and the combined effect of the Coriolis-Stokes force and Sm02 (CSFSm02, blue line). In panels (I)&(II), top (bottom) represents the bias for winter (summer) means.

smaller than CORA observations and is found to increase with Langmuir mixing and hence become closer to the observations. The smaller heat content in the control case is more pronounced in the subtropical and sub-polar gyre regions. This may be due to insufficient vertical mixing that reduces air-to-ocean heat fluxes, as these regions show warm SST bias in summer.

Except Van Roekel et al. (2012) and Li and Fox-Kemper (2017), all the other LT parameterizations apply a single enhancement factor for the velocity scale of both the eddy diffusivity and unresolved shear velocity. This approach is found to overestimate the winter MLD at

hight latitude (Fig. 4), and therefore it is more adequate to adopt separate enhancements for the two processes (e.g., Reichl et al., 2016b; Li and Fox-Kemper, 2017). Following the suggestion of Li et al. (2016), the surface Stokes drift is added to the unresolved shear in the bulk Richardson number (18) in the Van Roekel et al. (2012) experiment. However, in an experiment where we left out the surface Stokes drift from the unresolved shear (not shown) we found that its addition is actually detrimental to the MLD bias. Similar to Li and Fox-Kemper (2017), the modified unresolved shear velocity V_{tL}^2 (20) is found to magnify the LT effect under weak surface cooling and presence of wind

and wave, and to restrain it under strong/pure convective conditions. In addition, and because of its dependency on the ocean mixed layer, the surface layer averaged Langmuir number becomes small (magnifying the wave effects) during summer and large (suppressing the wave effects) during winter. This helps to constrain the winter mixing where the enhancement factor (21) approaches one, for example in deep convection regions such as the Labrador sea. Moreover, the surface layer averaged Langmuir number is better in capturing the effects from different wavelength and accurately predicts the value of the vertical turbulent kinetic energy (Harcourt and D'Asaro, 2008). Therefore, consideration of the Stokes penetration depth, hence the surface layer averaged Langmuir number (Harcourt and D'Asaro, 2008) and the stability Li and Fox-Kemper (2017) in the parameterized LT effects are important in restraining the excessive LT mixing, specially during winter.

Our results with respect to the impact with the scaling by McWilliams and Sullivan (2000) agree with findings in similar studies focused on global, climate time scale investigation of the impact of parameterized Langmuir turbulence on the boundary layer mixing such as Fan and Griffies (2014) and Li et al. (2016). Fan and Griffies (2014) argued that the too strong influence by the McWilliams and Sullivan (2000) scaling exaggerates the wave-induced turbulent mixing in weakly stratified winter conditions, and underestimates the mixing in stably stratified summer conditions. Therefore their choice was the Smyth et al. (2002) scheme finding it to perform better than MS00 for CM2 M with improvement in winter MLD around Labrador Seas.

It is worth noting that Li et al. (2016) reported a very high computational cost when using online wave-ocean coupling (36% increase in computer time). Like Li et al. (2017), our study demonstrates that off-line wave-ocean coupling, if wave forcing is available, can be an affordable approach to account for the Langmuir turbulence mixing and still introducing similar impacts.

The model control run without wave effects tends to exhibit both too shallow and too deep wintertime mixed layers at high latitudes, but the summertime MLD is almost everywhere underestimated. The LF17 parameterization yields the best performance in reducing these biases without degrading the existing MLD and SST results. There is probably still room for more improvement, for example the summertime Langmuir mixing is not strong enough to sufficiently deepen the mixed layer in the subtropical Atlantic ocean (30°N and 40°N). As shown in Fig. 10 in Reichl et al. (2016b), it is possible to increase the impact of LT mixing by considering the enhancement factor (21), but without taking the square root. It should be noted that the large biases in the control run (without wave mixing) cannot be attributed to missing LT effects. These shortcomings can be due to other physical processes that affect the mixing in the ocean boundary layer, as well as errors in the air-sea fluxes.

The comparisons of the different schemes are always consistent from one year to another. Moreover, the three years of simulation of the North Atlantic have experienced a wide variety of combinations of wave regimes and low/high heating of the ocean. The comparison of the temperature (SST and profiles) are made for the same three-year period as the observations, not from climatology. However, it would probably be interesting to extend the integration time and investigate the long-term impact.

Future work could couple the Langmuir mixing with re-stratification effects such as parameterization of meso- and sub-mesoscale eddies in the ocean boundary layer (Fox-Kemper et al., 2011). To reduce the excessive mixing in the control case Cntl, one may also consider adjusting the critical Richardson number, as it might have already been tuned to implicitly account for wave effects (Reichl et al., 2016b). Treating the latter as a free tuning parameter, a more fair comparison would have been achieved by adjusting a different value for each LT parameterization so that their median enhancement factor is equal. A more accurate assessment of the performance of LT parameterizations would also benefit from a different criterion for determining the MLD.

As reported by Noh et al. (2016) and Ok et al. (2017), the comparison of MLD diagnosed with the density threshold of 0.03 kg m^{-3} induces spurious errors at high latitudes during winter due to the different characteristics of the vertical density structures. Another potential extension would be to consider the LT parameterization by Reichl et al. (2016b), where two separate enhancement factors were suggested (including a dependency on the smooth function $G(z/h)$) for the velocity scale and the unresolved shear, which were derived using LES simulations under tropical cyclone conditions.

Further improvement can probably be achieved by including more wave parameters in the Langmuir turbulence parameterization such as the miss-alignment between the wind and wave directions (Van Roekel et al., 2012; McWilliams et al., 2014; Li et al., 2016). In this work, these effects have been neglected in Eqs. (17), (19) and (21).

McWilliams et al. (2014) and Reichl et al. (2016b) have shown the importance of including the Lagrangian shear in the parameterization of the turbulent momentum fluxes with LT. This is not considered here. The Lagrangian shear primarily affects the parameterization of the turbulent momentum flux in two ways. First by better aligning with the direction of the turbulent stress than when only using the Eulerian shear. This is however not an issue for us as KPP always imposes a current shear in the direction of the turbulent stress. The second effect is that the down-gradient mixing associated with Stokes drift shear will change the near surface Eulerian current, which may partially counter the Stokes advection term.

It is also supported by Sinha et al. (2015) who followed Teixeira (2012) and developed an LT parameterization for KPP that includes enhanced velocity scaling, non-local transport for momentum and local down-Stokes gradient mixing; which they have shown to give good results for full-depth Langmuir circulation in shallow water. Their results warrant future consideration of this parameterization in deep water. Another potentially important wave effect that can be investigated is a contribution of the Stokes shear force in the vertical momentum termed wavy hydrostatic by Suzuki and Fox-Kemper (2016). However, we expect departures from hydrostasy to be small in our model setup since the wavy hydrostatic Eq. (14) by Suzuki and Fox-Kemper (2016) differs from the hydrostatic equation by a term which scales with the Rossby number, which is small for basin scales.

We have performed a sensitivity study of the impact of several competing Langmuir parameterizations in a realistic basin-scale ocean model. The study provides upper and lower bounds on the impact that can be expected from including Langmuir parameterizations in KPP-type turbulence schemes. As expected, the MS00 parameterization is too strong, and indeed MS00 noted that the lack of a stability dependence would limit the usefulness of the parameterization in real settings. Overall the LT parameterizations exhibit a stronger impact in winter relative to summer, except the scheme by LF17 which induces summertime mixing stronger than that during winter, thus reducing summer temperature biases without degrading the winter SST. LF17 (Li and Fox-Kemper, 2017) thus stands out as the best-performing parameterization of the ones tested with this model setup and the only one which improves the overall biases compared with the model control run.

reviewers for their constructive comments, and also for insisting on us using the surface layer averaged Langmuir number. It was worth the effort.

References

Andrews, D.G., Mcintyre, M.E., 1978. An exact theory of nonlinear waves on a Lagrangian-mean flow. J. Fluid Mech. 89 (4), 609–646.

Antonov, J., Locarnini, R., Boyer, T., Mishonov, A., Garcia, H., 2006. World Ocean Atlas 2005. In: Levitus, S. (Ed.), Salinity. NOAA Atlas NESDIS, vol. 2. pp. 62.

Ardhuin, F., Jenkins, A.D., 2006. On the interaction of surface waves and upper ocean turbulence. J. Phys. Oceanogr. 36 (3), 551–557.

Ardhuin, F., Rascle, N., Belibassakis, K.A., 2008. Explicit wave-averaged primitive equations using a Generalized {L}agrangian Mean. Ocean Model. 20, 35–60.

Belcher, S.E., Grant, A.L.M., Hanley, K.E., Fox-Kemper, B., Van Roekel, L., Sullivan, P.P., Large, W.G., Brown, A., Hines, A., Calvert, D., Rutgersson, A., Pettersson, H., Bidlot, J.-R., Janssen, P.A.E.M., Polton, J.A., 2012. A global perspective on Langmuir turbulence in the ocean surface boundary layer. Geophys. Res. Lett. 39 (18).

Bennis, A.-C., Ardhuin, F., Dumas, F., 2011. On the coupling of wave and three-dimensional circulation models: choice of theoretical framework, practical implementation and adiabatic tests. Ocean Model. 40 (3-4), 260–272.

Bleck, R., 2002. An oceanic general circulation model framed in hybrid isopycnic-Cartesian coordinates. Ocean Model. 4 (1), 55–88.

Breivik, Ø., Bidlot, J.-R., Janssen, P.A.E.M., 2016. A Stokes drift approximation based on the Phillips spectrum. Ocean Model. 100, 49–56.

Breivik, Ø., Janssen, P., Bidlot, J.R., 2014. Approximate Stokes drift profiles in deep water. J. Phys. Oceanogr. 44 (9), 2433–2445.

Breivik, Ø., Mogensen, K., Bidlot, J.-R., Balmaseda, M.A., Janssen, P.A.E.M., 2015. Surface wave effects in the NEMO ocean model: forced and coupled experiments. J. Geophys. Res. Oceans 120 (4), 2973–2992.

Cabanes, C., Grouazel, A., von Schuckmann, K., Hamon, M., Turpin, V., Coatanoan, C., Paris, F., Guinehut, S., Boone, C., Ferry, N., de Boyer Montégut, C., Carval, T., Reverdin, G., Pouliquen, S., Le Traon, P.-Y., 2013. The CORA dataset: validation and diagnostics of in-situ ocean temperature and salinity measurements. Ocean Sci. 9 (1), 1–18.

Coatanoan, C., de la Villeon, L., 2005. In-situ data quality control procedures. In: Tech. rep. Ifremer report, pp. 17. http://www.coriolis.eu.org/content/download/4918/36060/file/cordo-rap-04-047-quality-control.pdf available at:.

Craik, A.D.D., Leibovich, S., 1976. A rational model for {L}angmuir circulations. J. Fluid Mech. 73, 401–426.

Danabasoglu, G., Large, W.G., Tribbia, J.J., Gent, P.R., Briegleb, B.P., McWilliams, J.C., 2006. Diurnal coupling in the tropical oceans of CCSM3. J. Clim. 19 (11), 2347–2365.

D'Asaro, E.A., Thomson, J., Shcherbina, A.Y., Harcourt, R.R., Cronin, M.F., Hemer, M.A., Fox-Kemper, B., 2014. Quantifying upper ocean turbulence driven by surface waves. Geophys. Res. Lett. 41 (1), 102–107.

de Boyer Montégut, C., Madec, G., Fischer, A.S., Lazar, A., Iudicone, D., 2004. Mixed layer depth over the global ocean: an examination of profile data and a profile-based climatology. J. Geophys. Res. Oceans 109 (C12).

Dee, D.P., Uppala, S.M., Simmons, A.J., Berrisford, P., Poli, P., Kobayashi, S., Andrae, U., Balmaseda, M.A., Balsamo, G., Bauer, P., Bechtold, P., Beljaars, A.C.M., van de Berg, L., Bidlot, J., Bormann, N., Delsol, C., Dragani, R., Fuentes, M., Geer, A.J., Haimberger, L., Healy, S.B., Hersbach, H., Hólm, E.V., Isaksen, L., Kållberg, P., Köhler, M., Matricardi, M., McNally, A.P., Monge-Sanz, B.M., Morcrette, J.J., Park, B.K., Peubey, C., de Rosnay, P., Tavolato, C., Thépaut, J.N., Vitart, F., 2011. The ERA-Interim reanalysis: configuration and performance of the data assimilation system. Q. J. R. Meteorol. Soc. 137 (656), 553–597.

Donlon, C.J., Martin, M., Stark, J., Roberts-Jones, J., Fiedler, E., Wimmer, W., 2012. The Operational Sea Surface Temperature and Sea Ice Analysis (OSTIA) system. Remote Sens. Environ. 116 (Supplement C), 140–158.

Drange, H., Simonsen, K., 1996. Formulation of air-sea fluxes in the ESOP2 version of MICOM. In: Tech. rep. Nansen Environmental and Remote Sensing Center, Thormøhlensgt. 47, N-5006 Bergen, Norway,.

Fan, Y., Griffies, S.M., 2014. Impacts of parameterized Langmuir turbulence and non-breaking wave mixing in global climate simulations. J. Clim. 27 (12), 4752–4775.

Fox-Kemper, B., Danabasoglu, G., Ferrari, R., Griffies, S.M., Hallberg, R.W., Holland, M.M., Maltrud, M.E., Peacock, S., Samuels, B.L., 2011. Parameterization of mixed layer eddies. III: implementation and impact in global ocean climate simulations. Ocean Model. 39 (1), 61–78.

Good, S.A., Martin, M.J., Rayner, N.A., 2013. EN4: quality controlled ocean temperature and salinity profiles and monthly objective analyses with uncertainty estimates. J. Geophys. Res. Oceans 118 (12), 6704–6716.

Grant, A.L.M., Belcher, S.E., 2009. Characteristics of Langmuir turbulence in the ocean mixed layer. J. Phys. Oceanogr. 39 (8), 1871–1887.

Griffies, S.M., Biastoch, A., Böning, C., Bryan, F., Danabasoglu, G., Chassignet, E.P., England, M.H., Gerdes, R., Haak, H., Hallberg, R.W., Hazeleger, W., Jungclaus, J., Large, W.G., Madec, G., Pirani, A., Samuels, B.L., Scheinert, M., Gupta, A.S., Severijns, C.A., Simmons, H.L., Treguier, A.M., Winton, M., Yeager, S., Yin, J., 2009. Coordinated Ocean-ice Reference Experiments (COREs). Ocean Model. 26 (1-2), 1–46.

Harcourt, R.R., D'Asaro, E.A., 2008. Large-eddy simulation of Langmuir turbulence in pure wind seas. J. Phys. Oceanogr. 38 (7), 1542–1562.

Hasselmann, K., 1970. Wave-driven inertial oscillations. Geophys. Fluid Dyn. 1, 463–502.

Hasselmann, K., 1971. On the Mass and Momentum Transfer Between Short Gravity Waves and Larger-Scale Motions. 4. pp. 189–205.

Janssen, P.A.E.M., 2012. Ocean wave effects on the daily cycle in SST. J. Geophys. Res. Oceans 117 (C11), 1–24.

Jenkins, A.D., 1989. The use of a wave prediction model for driving a near-surface current model. Dtsch. Hydrogr. Z. 42, 133–149.

Large, W.G., McWilliams, J.C., Doney, S.C., 1994. Oceanic vertical mixing: a review and a model with nonlocal boundary layer parameterization. Rev. Geophys. 32, 363–403.

Leibovich, S., 1983. The form and dynamics of Langmuir circulations. Annu. Rev. Fluid Mech. 15 (1), 391–427.

Li, M., Zahariev, K., Garrett, C., 1995. Role of Langmuir circulation in the deepening of the ocean surface mixed layer. Science 25, 1955–1957.

Li, Q., Fox-Kemper, B., 2017. Assessing the effects of Langmuir turbulence on the entrainment buoyancy flux in the ocean surface boundary layer. J. Phys. Oceanogr. 47 (12), 2863–2886.

Li, Q., Webb, A., Fox-Kemper, B., Craig, A., Danabasoglu, G., Large, W.G., Vertenstein, M., 2016. Langmuir mixing effects on global climate: WAVEWATCH III in CESM. Ocean Model. 103, 145–160.

Li, Q., Fox-Kemper, B., Breivik, Ø., Webb, A., 2017. Statistical models of global Langmuir mixing. Ocean Model. 113, 95–114.

Locarnini, R., Antonov, J., Garcia, H., 2006. World Ocean Atlas 2005. In: Levitus, S. (Ed.), Temperature. NOAA Atlas NESDIS, vol. 1. pp. 61.

McWilliams, J.C., Fox-Kemper, B., 2013. Oceanic wave-balanced surface fronts and filaments. J. Fluid Mech. 730, 464–490.

McWilliams, J.C., Huckle, E., Liang, J., Sullivan, P.P., 2014. Langmuir turbulence in swell. J. Phys. Oceanogr. 44, 870–890.

McWilliams, J.C., Restrepo, J.M., 1999. The wave-driven ocean circulation. J. Phys. Oceanogr. 29 (10), 2523–2540.

McWilliams, J.C., Restrepo, J.M., Lane, E.M., 2004. An asymptotic theory for the interaction of waves and currents in coastal waters. J. Fluid Mech. 511, 135–178.

McWilliams, J.C., Sullivan, P.P., 2000. Vertical mixing by Langmuir circulations. Spill Sci. Technol. Bull. 6 (3-4), 225–237.

McWilliams, J.C., Sullivan, P.P., Moeng, C.-H., 1997. Langmuir turbulence in the ocean. J. Fluid Mech. 334, 1–30.

Mellor, G., 2016, jun, jun. On theories dealing with the interaction of surface waves and ocean circulation. J. Geophys. Res. Oceans 121 (7), 4474–4486.

Noh, Y., Ok, H., Lee, E., Toyoda, T., Hirose, N., 2016. Parameterization of Langmuir circulation in the ocean mixed layer model using LES and its application to the OGCM. J. Phys. Oceanogr. 46 (1), 57–78.

Ok, H., Noh, Y., Choi, Y., 2017. Influence of pycnocline smoothing and subgrid-scale variability of density profiles on the determination of mixed layer depth. J. Atmos. Ocean. Technol. 34 (9), 2083–2101.

Phillips, O.M., 1958. The equilibrium range in the spectrum of wind-generated waves. J. Fluid Mech. 4 (4), 426–434.

Polton, J.A., Belcher, S.E., 2007. Langmuir turbulence and deeply penetrating jets in an unstratified mixed layer. J. Geophys. Res. Oceans 112 (C9).

Rascle, N., Ardhuin, F., 2013. A global wave parameter database for geophysical applications. Part 2: model validation with improved source term parameterization. Ocean Model. 70, 174–188.

Rascle, N., Ardhuin, F., Queffeulou, P., Croizé-Fillon, D., 2008. A global wave parameter database for geophysical applications. Part 1: wave-current-turbulence interaction parameters for the open ocean based on traditional parameterizations. Ocean Model. 25, 154–171.

Reichl, B.G., Ginis, I., Hara, T., Thomas, B., Kukulka, T., Wang, D., 2016a. Impact of sea-state-dependent Langmuir turbulence on the ocean response to a tropical cyclone. Mon. Weather Rev. 144 (12), 4569–4590.

Reichl, B.G., Wang, D., Hara, T., Ginis, I., Kukulka, T., 2016b. Langmuir turbulence parameterization in tropical cyclone conditions. J. Phys. Oceanogr. 46 (3), 863–886.

Rodgers, K.B., Aumont, O., Mikaloff Fletcher, S.E., Plancherel, Y., Bopp, L., de Boyer Montégut, C., Iudicone, D., Keeling, R.F., Madec, G., Wanninkhof, R., 2014. Strong sensitivity of Southern Ocean carbon uptake and nutrient cycling to wind stirring. Biogeosciences 11 (15), 4077–4098.

Rogers, W.E., Wallcraft, A.J., 2013. Develop and test coupled physical parameterizations and tripolar wave model grid: NAVGEM / WaveWatch III / HYCOM. In: Tech. Rep. Naval Research Laboratory, Stennis Space Center, MS 39529.

Saha, S., Moorthi, S., Pan, H.-L., Wu, X., Wang, J., Nadiga, S., Tripp, P., Kistler, R., Woollen, J., Behringer, D., et al., 2010. The NCEP climate forecast system reanalysis. Bull. Am. Meteorol. Soc. 91 (8), 1015–1057.

Sakov, P., Counillon, F., Bertino, L., Lisæter, K.A., Oke, P.R., Korablev, A., 2012. TOPAZ4: an ocean-sea ice data assimilation system for the North Atlantic and Arctic. Ocean Sci. 8 (4), 633–656.

Sallée, J.B., Shuckburgh, E., Bruneau, N., Meijers, A.J., Bracegirdle, T.J., Wang, Z., 2013. Assessment of Southern Ocean mixed-layer depths in CMIP5 models: historical bias and forcing response. J. Geophys. Res. Oceans 118 (4), 1845–1862.

Sheldon, L., Czaja, A., 2014. Seasonal and interannual variability of an index of deep atmospheric convection over western boundary currents. Q. J. R. Meteorol. Soc. 140 (678), 22–30.

Sinha, N., Tejada-Martinez, A.E., Akan, C., Grosch, C.E., 2015. Toward a K-profile parameterization of Langmuir turbulence in shallow coastal shelves. J. Phys. Oceanogr. 45 (12), 2869–2895.

Skagseth, Ø., Mork, K.A., 2012. Heat content in the Norwegian Sea, 1995–2010. ICES J. Mar. Sci. 69 (5), 826–832.

Skyllingstad, E.D., Denbo, D.W., 1995. An ocean large-eddy simulation of Langmuir circulations and convection in the surface mixed layer. J. Geophys. Res. 100, 8501–8522.

Smyth, W.D., Skyllingstad, E.D., Crawford, G.B., Wijesekera, H., 2002. Nonlocal fluxes and Stokes drift effects in the K-profile parameterization. Ocean Dyn. 52 (3), 104–115.

Stokes, G., 1847. On the theory of oscillatory waves. Trans. Cambridge Philos. Soc. 8, 441–455.

Sullivan, P.P., McWilliams, J.C., Melville, W.K., 2007. Surface gravity wave effects in the oceanic boundary layer: large-eddy simulation with vortex force and stochastic breakers. J. Fluid Mech. 593, 405–452.

Suzuki, N., Fox-Kemper, B., 2016. Understanding Stokes forces in the wave-averaged equations. J. Geophys. Res. Oceans 121 (5), 3579–3596.

Suzuki, N., Fox-Kemper, B., Hamlington, P.E., Van Roekel, L.P., 2016. Surface waves affect frontogenesis. J. Geophys. Res. Oceans 121 (5), 3597–3624.

Szekely, T., Gourrion, J., Pouliquen, S., Reverdin, G., 2016. CORA, Coriolis Ocean Dataset for Reanalysis. SEANOE https://doi.org/10.17882/46219.

Takaya, Y., Bidlot, J.-R., Beljaars, A.C.M., Janssen, P.A.E.M., 2010. Refinements to a prognostic scheme of skin sea surface temperature. J. Geophys. Res. Oceans 115 (C6).

Teixeira, M.A.C., 2012. The influence of Langmuir turbulence on the scaling for the dissipation rate in the oceanic boundary layer. J. Geophys. Res. Oceans 117 (C5).

Thorpe, S.A., 2004. Langmuir circulation. Annu. Rev. Fluid Mech. 36 (1), 55–79.

Tolman, H.L., Balasubramaniyan, B., Burroughs, L.D., Chalikov, D.V., Chao, Y.Y., Chen, H.S., Gerald, V.M., 2002. Development and implementation of wind-generated ocean surface wave models at NCEP. Weather Forecast. 17 (2), 311–333.

Tolman, H.L., Others, 2009. User manual and system documentation of WAVEWATCH III TM version 3.14. In: Tech. Rep. 276. MMAB/NCEP/NOAA.

Uchiyama, Y., McWilliams, J.C., Shchepetkin, A.F., 2010. Wave-current interaction in an oceanic circulation model with a vortex-force formalism: application to the surf zone. Ocean Model. 34 (1-2), 16–35.

Uotila, P., Goosse, H., Haines, K., Chevallier, M., Barthélemy, A., Bricaud, C., Carton, J., Fučkar, N., Garric, G., Iovino, D., Kauker, F., Korhonen, M., Lien, V.S., Marnela, M., Massonnet, F., Mignac, D., Peterson, K.A., Sadikni, R., Shi, L., Tietsche, S., Toyoda, T., Xie, J., Zhang, Z., 2018. An assessment of ten ocean reanalyses in the polar regions. Clim. Dyn. 1–38.

van den Bremer, T.S., Breivik, Ø., 2018. Stokes drift. Philos. Trans. R. Soc. Lond. A 376, 23.

Van Roekel, L.P., Fox-Kemper, B., Sullivan, P.P., Hamlington, P.E., Haney, S.R., 2012. The form and orientation of Langmuir cells for misaligned winds and waves. J. Geophys. Res. Oceans 117 (C5).

Weber, J.E., 1983. Steady wind- and wave-induced currents in the open ocean. J. Phys. Oceanogr. 13 (3), 524–530.

Weber, J.E.H., Broström, G., Saetra, Ø., 2006. Eulerian versus Lagrangian approaches to the wave-induced transport in the upper ocean. J. Phys. Oceanogr. 36 (11), 2106–2118.

Williams, K.D., Copsey, D., Blockley, E.W., Bodas-Salcedo, A., Calvert, D., Comer, R., Davis, P., Graham, T., Hewitt, H.T., Hill, R., Hyder, P., Ineson, S., Johns, T.C., Keen, A.B., Lee, R.W., Megann, A., Milton, S.F., Rae, J.G., Roberts, M.J., Scaife, A.A., Schiemann, R., Storkey, D., Thorpe, L., Watterson, I.G., Walters, D.N., West, A., Wood, R.A., Woollings, T., Xavier, P.K., 2018. The Met Office Global Coupled Model 3.0 and 3.1 (GC3.0 and GC3.1) configurations. J. Adv. Model. Earth Syst. 10 (2), 357–380.

Zeng, X., Beljaars, A., 2005. A prognostic scheme of sea surface skin temperature for modeling and data assimilation. Geophys. Res. Lett. 32: L14605 (14).